Article

Cell Reports

Control of Intestinal Cell Fate by Dynamic Mitotic Spindle Repositioning Influences Epithelial Homeostasis and Longevity

Graphical Abstract

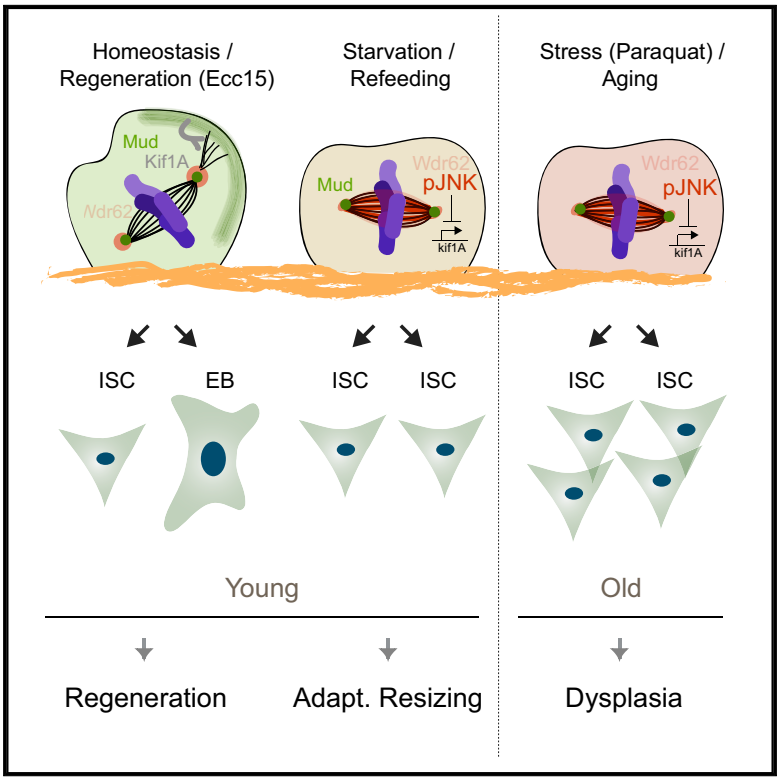

Authors

Daniel Jun-Kit Hu, Heinrich Jasper

Correspondence

hud10@gene.com (D.J.-K.H.),
jasperh@gene.com (H.J.)

In Brief

Hu and Jasper demonstrate that spindle orientation regulates stem cell fate in *Drosophila* intestines. JNK activity promotes reorientation from oblique to planar spindles, increasing symmetric outcomes. This switch is required for growth but becomes chronic during stress and age. Restoring oblique spindles in old animals improves tissue physiology, extending lifespan.

Highlights

- Spindles reorient from oblique to planar during growth, driving symmetric outcomes
- Stress- and aging-mediated activation of JNK promotes planar spindles
- JNK interacts with Wdr62 and represses Kif1a expression to promote planar spindles
- Restoring oblique spindles in old flies extends lifespan

Hu & Jasper, 2019, Cell Reports *28*, 2807–2823
September 10, 2019
https://doi.org/10.1016/j.celrep.2019.08.014

CellPress

Cell Reports
Article

Control of Intestinal Cell Fate by Dynamic Mitotic Spindle Repositioning Influences Epithelial Homeostasis and Longevity

Daniel Jun-Kit Hu[1,*] and Heinrich Jasper[1,2,3,*]
[1]Genentech Inc., 1 DNA Way, South San Francisco, CA 94080, USA
[2]The Buck Institute for Research on Aging, 8001 Redwood Boulevard, Novato, CA 94945, USA
[3]Lead Contact
*Correspondence: hud10@gene.com (D.J.-K.H.), jasperh@gene.com (H.J.)
https://doi.org/10.1016/j.celrep.2019.08.014

SUMMARY

Tissue homeostasis depends on precise yet plastic regulation of stem cell daughter fates. During growth, *Drosophila* intestinal stem cells (ISCs) adjust fates by switching from asymmetric to symmetric lineages to scale the size of the ISC population. Using a combination of long-term live imaging, lineage tracing, and genetic perturbations, we demonstrate that this switch is executed through the control of mitotic spindle orientation by Jun-N-terminal kinase (JNK) signaling. JNK interacts with the WD40-repeat protein Wdr62 at the spindle and transcriptionally represses the kinesin Kif1a to promote planar spindle orientation. In stress conditions, this function becomes deleterious, resulting in overabundance of symmetric fates and contributing to the loss of tissue homeostasis in the aging animal. Restoring normal ISC spindle orientation by perturbing the JNK/Wdr62/Kif1a axis is sufficient to improve intestinal physiology and extend lifespan. Our findings reveal a critical role for the dynamic control of SC spindle orientation in epithelial maintenance.

INTRODUCTION

In many tissues, somatic stem cells (SCs) maintain regenerative capacity. SC population size and proliferative activity are tightly regulated to ensure effective regenerative responses to damage, without causing ectopic growth. Processes to expand or restore SC populations have been described in various tissues and may be evolutionarily conserved (O'Brien et al., 2011; Tata et al., 2013; Yan et al., 2017). These processes include de-differentiation of differentiated cells into tissue SCs (Lucchetta and Ohlstein, 2017; Tata et al., 2013; Tetteh et al., 2016; Tian et al., 2011), as well as changes in SC division modes (O'Brien et al., 2011). SC division modes in which both daughter cells become SCs (symmetric outcomes) can increase the proportion of SCs in the tissue, whereas division modes in which SCs self-renew and generate a differentiating daughter cell (asymmetric outcomes) maintain a homeostatic balance of SCs to differentiated cells (Keyes and Fuchs, 2018; Morrison and Spradling, 2008; Venkei and Yamashita, 2018). The ratio of symmetric to asymmetric outcomes must be carefully regulated to properly respond to environmental perturbations and maintain homeostasis.

Intestinal stem cell (ISC) divisions in *Drosophila* represent an ideal model system to study the regulation of SC division modes during regeneration, growth, damage, and aging. The *Drosophila* intestine is lined with a pseudo-stratified epithelium that is regenerated by ISCs after damage to ensure tissue function (Buchon et al., 2009b; Micchelli and Perrimon, 2006; Ohlstein and Spradling, 2006). Delta (D1)-expressing ISCs give rise to either enteroblasts (EBs), which terminally differentiate into enterocytes (ECs), or enteroendocrine cells (EEs) (Li and Jasper, 2016; Micchelli and Perrimon, 2006; Ohlstein and Spradling, 2006). These asymmetric ISC divisions are predominant during homeostasis, but in periods of growth, most ISC division modes can change to lead to symmetric outcomes, increasing the number of ISCs (O'Brien et al., 2011). This switch in division modes is critical to ensure appropriate epithelial cell composition. During aging, and in response to excessive oxidative stress, ISC proliferation and differentiation become deregulated, and the number of D1-expressing cells increases substantially, reflecting a possible mis-regulation in the switch from asymmetric to symmetric fates (Biteau et al., 2008). The molecular and cellular mechanisms executing this switch have not yet been elucidated.

The cell fate of many dividing cell types during development, ranging from *Drosophila* neuroblasts to mammalian radial glial and epidermal basal cells, is determined by spindle orientation during mitosis (Lancaster and Knoblich, 2012; Lechler and Fuchs, 2005; Morin and Bellaïche, 2011; Siller and Doe, 2009). In these cells, cell polarity and spindle orientation are tightly linked, and a complex composed of polarized cortical proteins (Baz/Par3, Par6, and aPKC) aligns the mitotic spindle during asymmetric division through the interaction of cytoplasmic dynein with a series of scaffolding proteins (Insc, Pins/LGN, and Mud/NuMA) (Bellaïche et al., 2001; Costa et al., 2008; Hao et al., 2010; Wodarz et al., 1999). In *Drosophila* neuroblasts, cell fate determinants promoting differentiation are then segregated along the apical-basal axis into the two daughter cells during anaphase to drive cell fate specification (Doe et al., 1991; Knoblich et al., 1995; Shen et al., 1997). Although the role of spindle orientation in driving symmetric versus asymmetric divisions is conserved among many developing epithelial tissues (Siller and Doe, 2009; Williams and Fuchs, 2013), in adult tissue, the

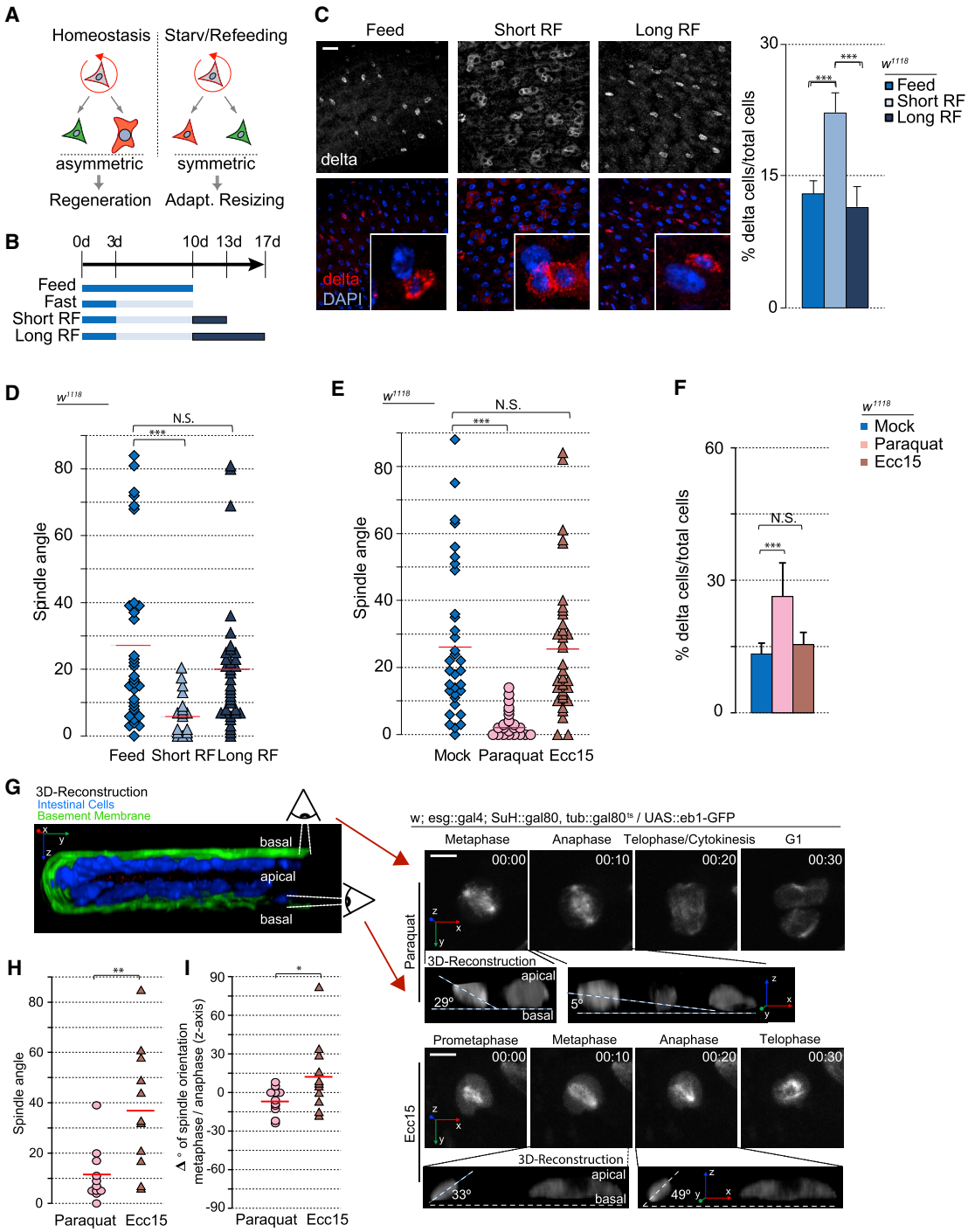

Figure 1. Spindle Orientation Responds to Different Environmental Perturbations

(A) Diagram representing different modes of ISC division in response to different environmental challenges.

(B) Timeline of fasting and refeeding conditions.

(C) Percentage of D1+ cells (ISCs) increased after short-term refeeding but returned to baseline levels after long-term refeeding. Insets depict a likely clone.

(D and E) Quantification of spindle orientation after refeeding conditions (D) and Paraquat treatment versus *Ecc15* infection (E).

(F) Percentage of D1+ cells increased after paraquat treatment, but not after *Ecc15* infection.

(G) Intestines imaged live *ex vivo* (hours:minutes). Insets depict 3D reconstruction.

(H) Spindle orientation in live ISCs mimicked that of fixed cells.

(I) Changes in spindle orientation between metaphase and anaphase.

(legend continued on next page)

role of spindle orientation during cell fate specification remains unclear. In the adult *Drosophila* intestine, the spindle orientation of dividing ISCs has been implicated in controlling fate specification (Goulas et al., 2012), but the extent to which spindle orientation affects fate is unclear and controversial: a role for integrins has been proposed to determine spindle orientation and promote asymmetric segregation of Par3, Par6, and aPKC, resulting in asymmetric activation of Notch in the two daughter cells (Goulas et al., 2012), while other studies have observed an initial symmetric segregation of D1 and Notch in the two daughter cells and repression of Notch target genes in ISCs to preserve their identity (Bardin et al., 2010; Li and Jasper, 2016; Micchelli and Perrimon, 2006; Ohlstein and Spradling, 2006). These models are not mutually exclusive, yet a deeper understanding of the dynamics of spindle orientation and cell fate is critical.

Here, we demonstrate that SC spindle orientation and cell fate in the adult *Drosophila* intestine are tightly linked. We find that transient Jun-N-terminal kinase (JNK) activation promotes the symmetric outcome of ISC divisions during intestinal growth. JNK regulates spindle orientation both directly, through recruitment of Wdr62 to the spindle, and transcriptionally, by repressing the expression of Kif1a (Unc-104), a kinesin implicated in promoting asymmetric divisions in rat radial glial cells (Carabalona et al., 2016). Chronic activation of this regulatory process by stress and aging results in cell fate defects by orienting ISC spindles planar to the basal surface. Accordingly, restoring normal spindle orientation in aging and stress conditions restores normal cell fates, preserves the barrier function of the intestine, and increases overall longevity. Our results deepen our understanding of cell fate regulation in barrier epithelia and identify potential intervention strategies toward preserving long-term tissue homeostasis.

RESULTS

Dynamic Spindle Orientation in Intestinal Stem Cells

To gain deeper insight into the cellular mechanisms controlling ISC cell fate, we asked whether the previously described switch from asymmetric to symmetric lineages during adaptive tissue resizing (O'Brien et al., 2011) (Figure 1A) would be reflected in the spindle orientation of mitotic ISCs. We induced adaptive resizing by fasting flies for a week, followed by refeeding (Figure 1B). The low-level mitotic activity observed in the intestine of normally fed flies in homeostasis (quantified by phospho-histone H3 [PH3] staining) declined after 7 days of protein deprivation on 1% sucrose (fasting) (Figure S1A) but was restored after a 3-day refeeding period (short-term refeeding). Consistent with this fluctuation in mitotic activity, intestinal size decreased after fasting but returned to normal after refeeding for 7 days (long-term refeeding) (Figure S1B). Consistent with previous studies (O'Brien et al., 2011), these changes in intestinal size were accompanied by an increase in the percentage (relative numbers) of ISCs, as determined by D1 expression after 3 days of refeeding and a return to normal levels after 7 days (Figure 1C). These transient feeding-induced changes in Dl+ cell numbers have been described as a consequence of transitions between symmetric and asymmetric outcomes (O'Brien et al., 2011). To test whether they are accompanied by changes in mitotic spindle orientation, we performed immunostaining against α- and γ-tubulin (microtubules and centrosomes, respectively) and assessed spindle orientation in relation to the basement membrane by using 3D reconstruction (Figures 1D and S1C–S1E). The orientation of the epithelial basement membrane was visualized either using Viking-GFP (a protein-trap line reporting expression of the *Drosophila* collagen Viking) (Buszczak et al., 2007) or using fluorescently tagged phalloidin (which visualizes the visceral muscle underlying the basement membrane) (Figures S1D and S1E). Consistent with previous reports (Goulas et al., 2012; Ohlstein and Spradling, 2007), mitotic ISCs in homeostatic conditions displayed both planar spindles ($\sim$0°–15° relative to the basement membrane) and widely distributed, oblique spindle angles (Figure 1D). After short-term refeeding, however, nearly all ISC spindles were planar. After long-term refeeding, spindles returned to a mix of planar and oblique orientations, suggesting that spindle orientation responds dynamically to growth cues and may be associated with the change from asymmetric to symmetric outcomes.

We asked whether dynamic ISC spindle reorientation would also be observed during damage-induced regeneration by infecting flies with *Erwinia carotovora carotovora 15* (*Ecc15*), a gram-negative bacterium that damages differentiated enterocytes and induces a rapid but controlled regenerative response in the *Drosophila* intestine, before being cleared from the gut (Ayyaz and Jasper, 2013; Buchon et al., 2009b). *Ecc15* exposure increased mitotic activity (Figure S1F) but did not affect spindle orientation or relative D1+ cell numbers substantially from homeostatic conditions (Figure 1E), suggesting that oblique spindles are preferred for regenerative conditions, in which predominantly asymmetric outcomes of ISC divisions are necessary.

However, we observed a significant shift in ISC spindle orientation when subjecting flies to more severe stress conditions. Oxidative stress triggered by exposure to paraquat induces a well-described response that is long lasting, resulting in dysplastic epithelial phenotypes reminiscent of age-related epithelial dysfunction (Biteau et al., 2008). In these conditions, ISC proliferation was also increased, but spindles reoriented planar relative to the basement membrane (Figure 1E). Paraquat exposure also led to an increase in relative numbers of Dl+ cells, suggesting a symmetric outcome of these divisions (Figures 1F and S1G). In these conditions, the relative numbers of fully differentiated cell types (ECs and EEs) in the epithelium decreased (Figure S5A).

Spindle Orientation Determines Symmetric versus Asymmetric Fate Specification

Our quantifications of Dl+ cells in different conditions indicated that changes in spindle orientation correlate with changes

Mean ± SD (C and F); n = 9 flies (C and F) and n = 11 cells from 6 flies (H and I), with spindle orientation quantified from 15–30 flies (D and E); N.S., not significant; *p < 0.05, **p < 0.01, ***p < 0.001, based on a Kruskal-Wallis test (C–F) or Mann-Whitney test (H and I). Red bar, mean (D, E, H, and I). Scale bars, 20 μm (C) and 5 μm (G).
See also Figure S1 and Videos S1 and S2.

between symmetric and asymmetric outcomes of ISC divisions. To test this, we first explored the kinetics of spindle dynamics in real time, visualizing spindle orientation dynamics using an *ex vivo* culture system for the fly intestine (Deng et al., 2015). We imaged mitotic events in live intestines of flies expressing a GFP-tagged version of the microtubule plus-end tracking protein EB1 in ISCs (Figures 1G and 1H) (Rogers et al., 2002). EB1-GFP labels the mitotic spindle throughout M phase, allowing dynamic tracking of spindle orientations (Figure 1H; Videos S1 and S2). In response to *Ecc15* exposure, the spindle often rotated between metaphase and anaphase, suggesting dynamic realignment of the spindle during mitosis (Figures 1G and 1H), similar to observations in homeostasis (Martin et al., 2018). This rotation was less common and dramatic after paraquat treatment and resulted in a more planar spindle orientation during anaphase, consistent with our observations in fixed tissue. We also measured spindle orientation in live tissue after short-term refeeding and observed largely planar spindles with minimal rotation (Figure S1H).

To ask whether the observed changes in spindle orientation correlate with fate switches in the ISC lineage, we performed twin-spot mosaic analysis (Yu et al., 2009). In this approach, the two daughter cells of an ISC division are differentially labeled with GFP or RFP. Subsequent lineage tracing of each daughter cell then allows retroactive specification of the fate of the two cells (Figures 2A and S2). ISCs from flies exposed to either mock treatment or *Ecc15* infection exhibited largely asymmetric divisions (resulting in lineages in which all cells were given the same color, because the differently labeled daughter cell differentiates and is eventually shed without generating a labeled clone of cells), confirming the asymmetric outcome of divisions with oblique spindle orientations (Figure 2A). Paraquat treatment, in turn, resulted in largely symmetric divisions, as represented by closely associated cell clones in different colors. Short-term refeeding also resulted in largely symmetric divisions, consistent with the observed shift from oblique to planar spindles (Figures 1D and 2A). Similarly correlating with a return to oblique spindles, we observed largely asymmetric divisions after long-term refeeding.

To establish causality between spindle orientation and cell fate in the ISC lineage, it is essential to directly visualize the connection between spindle orientation and SC division outcome. We devised an *ex vivo* system to capture mitotic ISCs and measure spindle orientation while following the cell fate of daughter cells. Enhanced yellow fluorescent protein (eYFP) is expressed specifically and inducibly in ISCs using the Temporal and Regional Gene Expression Targeting (TARGET) system, involving the ISC/EB driver *escargot::Gal4* in combination with the EB-specific expression of the Gal4 inhibitor Gal80 (Su(H)::Gal80) (Wang et al., 2014) and ubiquitous expression of temperature-sensitive Gal80 (tub::Gal80^{ts}) (McGuire et al., 2004). A daughter EB is identified by mCherry driven by the Su(H) promoter. As such, asymmetric division generates a YFP+/mCherry+ cell and a YFP+ cell, while symmetric division generates two YFP+/mCherry− cells (Figures 2C, S3, S4A, and S4B; Videos S3, S4, S5, S6, S7, and S8). After an asymmetric outcome, mCherry fluorescence was, on average, initially visible in one of the daughter cells 8 h post-mitosis before increasing in intensity throughout the time lapse (Figure S4B). Symmetric outcomes were only scored at the end of the time lapse, averaging 12 h post-mitosis (Figure S4B).

We followed ISC daughter cells, determined their fate, and then retroactively measured spindle orientation. Neighboring stem cells line the basement membrane and were used to estimate its location, whereas the spindle was estimated by measuring the vector bisecting the two segregating cell bodies (Figures 2B, 2C, S3, and S4C). All asymmetric lineages were generated from oblique spindles (>15°; n = 12/12), and nearly all symmetric lineages were generated from planar spindles ($\leq$15°; n = 32/34) (Figures 2B, 2C, and S3). Consistent with previous observations, spindles were mostly oblique after *Ecc15* infection, whereas spindles were mostly planar after paraquat treatment or short-term refeeding (Figure S1C) (homeostatic conditions were not examined, because mitotic events are rare).

Altogether, these data support the idea that changes in spindle orientation are associated with the transition from asymmetric to symmetric SC outcomes in the adult *Drosophila* intestine. Excessive stress seems to prevent the acquisition of oblique spindles and thus result in disproportionate amounts of symmetric divisions. We hypothesized that stress-induced regulators of ISC activity may be involved in the physiological control of ISC spindle orientation to promote excessive symmetric fate specifications. To test this hypothesis, we asked whether JNK signaling may be influencing ISC spindle orientation.

Activation of the JNK Pathway Promotes Planar Spindle Orientation

The JNK pathway is evolutionarily conserved and induces ISC divisions in response to stress, including paraquat, through both cell-autonomous mechanisms (Biteau et al., 2008, 2010) and non-autonomous mechanisms (Jiang et al., 2009; Patel et al., 2015). Chronic or excessive activation of JNK can lead to epithelial dysplasia that is characterized by ISC overproliferation and the excessive production of Dl+ cells (Biteau et al., 2008). The mitotic response to JNK activation is mediated by the transcription factor Fos (Biteau et al., 2011), yet how JNK promotes the excess production of Dl+ cells remains unclear.

We assessed the presence of phosphorylated JNK (pJNK) in mitotic ISCs under varying conditions using immunohistochemistry with a previously described antibody that cross-reacts with *Drosophila* pJNK (Igaki et al., 2009; Wang et al., 2014). As expected, pJNK could not be detected in mitotic ISCs under homeostasis (in normally fed animals) (Figures 3A and S5D). After fasting and short-term refeeding and paraquat treatment, however, pJNK was detected at the mitotic spindle in dividing ISCs. This signal was not observed after long-term refeeding or in *Ecc15*-infected animals (Figures 3A and S5D). The difference in JNK activity in ISCs of *Ecc15*- and paraquat-exposed animals is consistent with the notion that *Ecc15* infection is a less severe and transient form of stress, whereas paraquat exposure leads to significant and long-lasting oxidative stress. Consistently, paraquat resulted in long-lasting epithelial dysplasia (characterized by increases in PH3+ cell numbers and in D1+ cell numbers) that was observed even 24 h after transferring flies to normal food (Figures S5B and S5C). In contrast, both PH3+ and D1+ cell numbers returned to baseline numbers after a 24-h recovery from *Ecc15* infection.

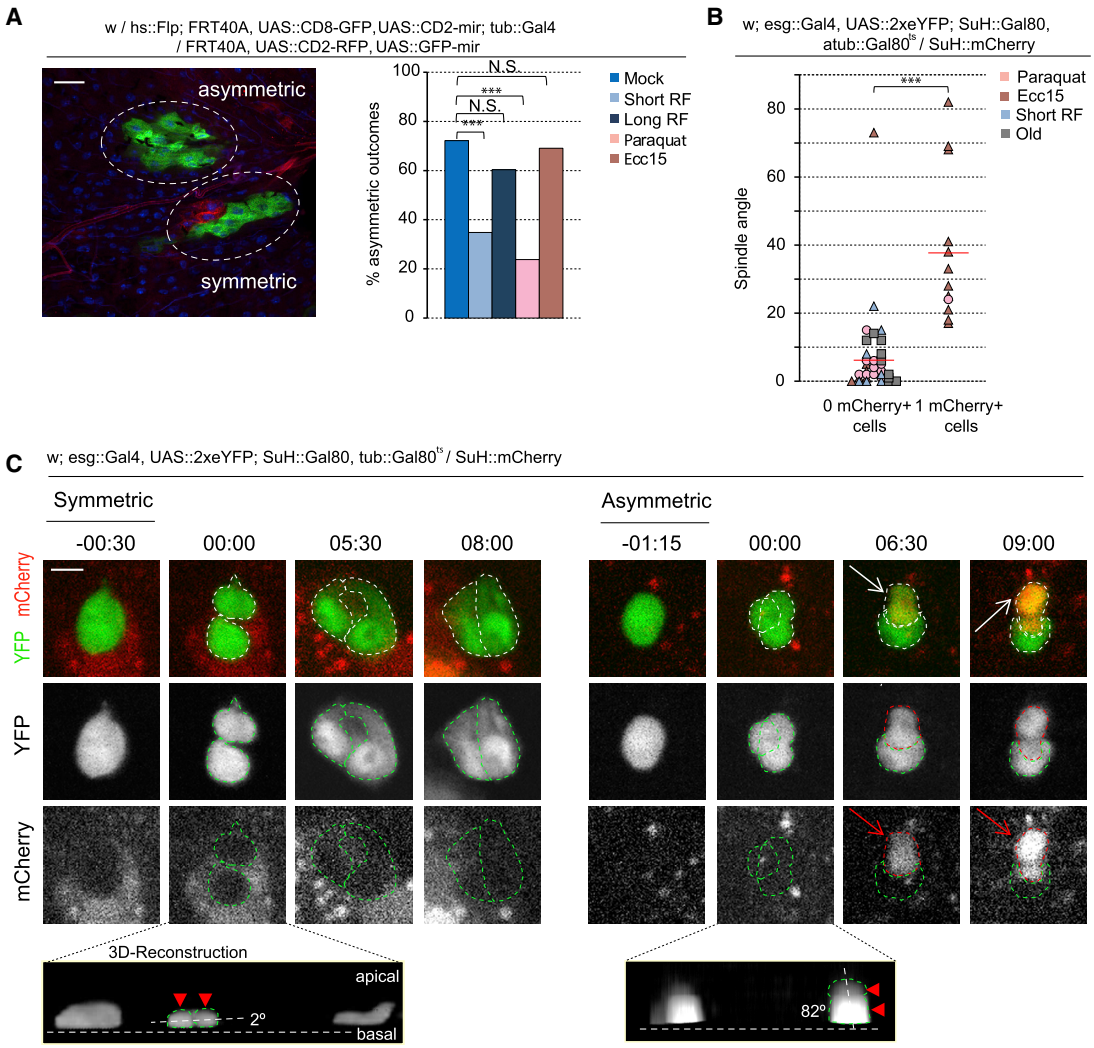

Figure 2. Spindle Orientation Is an Indicator of Cell Fate

(A) Quantification and representative image of twin-spot clones.

(B and C) Quantification (B) and montage (C) of symmetric versus asymmetric outcomes after live imaging of *ex vivo* intestines. Telophase-cytokinesis was set at 00:00 (hours:minutes). During a symmetric outcome, the dividing cell (−00:30–00:00) forms two daughter cells that remain mCherry− for the duration of the video (08:00). During an asymmetric outcome, the dividing cell (−01:15–00:00) forms two daughter cells. One of the daughter cells remains mCherry−, whereas the other daughter cell becomes mCherry+ (arrow, 06:30). Cell bodies are outlined with green for mCherry− and red for mCherry+. Insets depict 3D reconstruction of the two segregating cell bodies (arrowhead and outlined).

Mean ± SD; n = 133 (young), 112 (short-term refeed), 63 (long-term refeed), 42 (paraquat), and 84 (*Ecc15*) clones from ≥10 flies per condition (A), with spindle orientation quantified from 26 flies (B); N.S., not significant; ***$p < 0.001$, based on a chi-square test (A) or Mann-Whitney test (B). Red bar, mean (B). Scale bars, 20 μm (A) and 5 μm (C).

See also Figures S2–S4 and Videos S3, S4, S5, S6, S7, and S8.

Because the recruitment of pJNK to the spindle correlated with the reorientation of spindles, we asked whether JNK activity controlled spindle orientation. Using the TARGET system (Wang et al., 2014), we activated JNK inducibly and specifically in ISCs, either by overexpressing JNK (*Drosophila* hemipterous [Hep]) or by knocking down *puckered* (*puc*), which encodes a JNK phosphatase (Jiang et al., 2011; Martín-Blanco et al., 1998; Nam et al., 2012; Wang et al., 2003). Overactivating JNK in ISCs shifted spindles toward planar orientations and increased the relative numbers of D1+ cells, phenocopying growth and stress conditions (Figures 3B and 4E). Long-term live lineage tracing experiments revealed that depletion of Puc resulted in only symmetric lineages (all of which were derived from planar spindles) (Figure 4F). Conversely, disrupting the JNK pathway in ISCs by expressing a kinase-dead, dominant-negative form of the *Drosophila* JNK Basket (Bsk^{DN}) (Jasper et al., 2001) prevented the shift to planar orientation after paraquat treatment (Figure 3B) (this did not cause apoptosis, as determined by cleaved caspase-3 staining; Figures S6B and S6C). Expression of Bsk^{DN} also prevented the

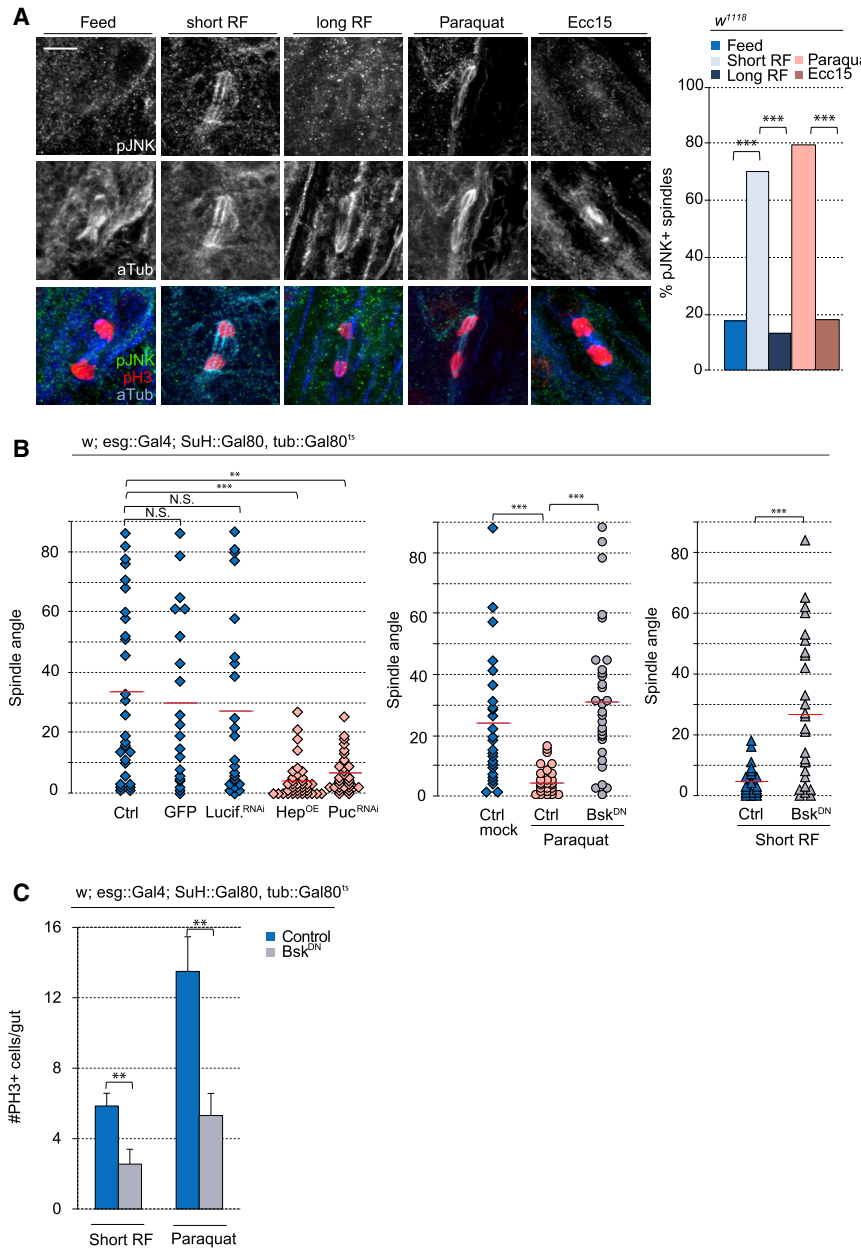

Figure 3. JNK Activity Promotes Planar Spindle Orientation

(A) Triple staining with anti-phosphorylated-JNK (pJNK), anti-phospho-histone H3 (PH3), and anti-α-tubulin revealed pJNK localization at the spindle after paraquat or short-term refeeding.

(B) Quantification of spindle orientation.

(C) Quantification of mitotic ISCs in whole gut after Bsk^{DN} expression.

Mean ± SEM (C); n ≥ 20–28 cells from ≥16 flies (A), n = 9 flies (Bsk^{DN} Short RF), or n ≥ 16 flies (C), with spindle orientation quantified from 18–35 flies per condition (B); N.S., not significant; **p < 0.01, ***p < 0.001, based on a chi-square test (A), Kruskal-Wallis test (B), or Mann-Whitney test (C). Red bar, mean (B). Scale bar, 5 μm.

See also Figure S5.

JNK Biases Symmetric Lineages by Decreasing Kif1a-Mediated Spindle Orientation

JNK can regulate cell function by phosphorylating transcription factors to change the transcriptome. We asked whether JNK-dependent changes in spindle orientation may also be influenced in part by the transcriptional induction or repression of selected target genes. We previously explored the transcriptome of isolated ISCs from intestines exposed to tunicamycin, which triggers JNK activation in ISCs (Wang et al., 2014, 2015). Although the expression of scaffolding proteins involved in recruiting the spindle (Baz, Insc, Pins, and Mud) during asymmetric divisions was largely unaffected, Kif1a, a kinesin reported to promote asymmetric divisions in embryonic neural stem cells (Carabalona et al., 2016), was downregulated more than 4-fold (Wang et al., 2014, 2015). Confirming this, qPCR on RNA extracted from fluorescence-activated cell sorting (FACS)-sorted ISCs revealed a 6-fold decrease in Kif1a RNA levels after

shift to planar orientation during short-term refeeding, confirming that JNK activation is required for the dynamic change in spindle orientation during adaptive resizing. Expression of luciferase double-stranded RNA (dsRNA) or cytoplasmic GFP alone did not affect spindle orientation (Figure 3B). Consistent with previous observations that increasing JNK activity increased mitotic activity (Biteau et al., 2008), we found that conversely, disrupting JNK activity using Bsk^{DN} expression was sufficient to decrease mitotic events in paraquat-treated or short-term refed animals (Figure 3C). Altogether, our results suggest that the association of phosphorylated JNK with the spindle is critical for the reorientation of mitotic spindles in ISCs during stress conditions and adaptive resizing.

increasing JNK activity by knocking down *puc* (Figure 4A). To assess whether this repression of Kif1a would contribute to the JNK-induced changes in spindle orientation, we tested the effect of Kif1a knockdown on spindle orientation of ISCs. Depleting Kif1a increases planar spindles while overexpressing Kif1a rescues the shift in planar spindle orientation caused by paraquat or *puc* depletion (Figures 4B, 4C, and S6G). Kif1a-mediated rescue of oblique spindles in paraquat-treated intestines was also observed with live imaging (Figure S6A). Kif1a overexpression did not significantly affect spindle orientation in conditions in which JNK was not activated (Figure 4B). These data suggest that Kif1a repression is required downstream of JNK activation to promote planar spindles. Accordingly, the percentage of

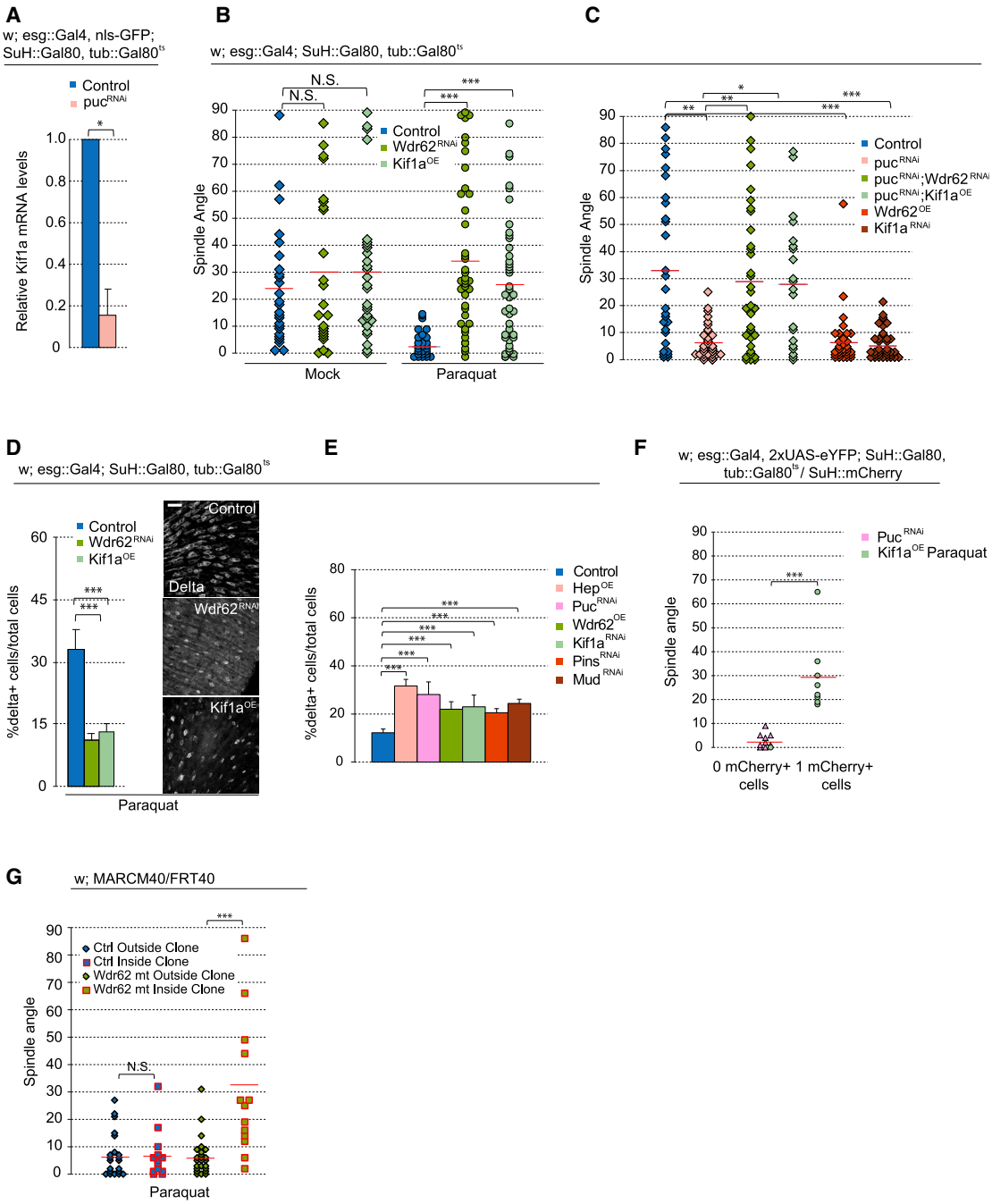

Figure 4. Wdr62 RNAi and Kif1a Overexpression Rescues Stressed-Induced Effects on Spindle Orientation

(A) Relative mRNA levels of Kif1a, normalized to Actin5c, in ISCs were decreased after *puc*^{RNAi}.

(B and C) Quantification of spindle orientation after genetic perturbation. Expressing full-length Kif1a or Wdr62^{RNAi} prevented the shift to planar spindles normally observed after Paraquat (B) or *puc*^{RNAi} (C). Untreated, mock-treated, and paraquat-treated *puc*^{RNAi} control data and were taken from Figure 3B, because experiments were done in parallel.

(D and E) Quantification of the percentage of D1+ cells after expressing full-length Kif1a or Wdr62^{RNAi} in Paraquat-treated flies (D) or after genetic perturbations that promoted planar spindles (E).

(F) Long-term live imaging lineage tracing experiments revealed that Puc^{RNAi} generated symmetric lineages, whereas expressing full-length Kif1a in paraquat-treated flies gave rise to asymmetric lineages.

(G) *wdr62* loss of function restored oblique spindles despite paraquat treatment.

(legend continued on next page)

D1+ cells increased after Kif1a knockdown, while in paraquat-treated intestines, the percentage of ISCs decreased after Kif1a overexpression, consistent with increased asymmetric divisions after promoting oblique spindles (Figures 4D and 4E). We ruled out the possibility of mitotic arrest and apoptosis affecting ISC numbers, observing that all mitoses in Kif1a-overexpressing ISCs from live-imaged guts continued to completion (n = 21 cells), and overexpressing Kif1a did not affect the mitotic index or increase the number of cleaved caspase-3+ ISCs (Figures S6C and S6D; Video S9). We performed long-term live lineage tracing experiments to directly test whether preventing the shift to planar spindles in paraquat-treated intestines would restore asymmetric outcomes. After Kif1a overexpression, 8/9 observed divisions were asymmetric, even after paraquat exposure (Figure 4F).

JNK Is Recruited to ISC Spindle by Wdr62 to Promote Planar Spindles

A role for JNK signaling in modulating spindle orientation has previously been described in the developing mammalian neocortex, in which JNK was shown to be recruited to the spindle of mitotic radial glial cells by the WD40-repeat protein Wdr62 (Xu et al., 2014). Wdr62 is a centrosome-associated protein and a phosphorylation target of JNK (Bogoyevitch et al., 2012; Cohen-Katsenelson et al., 2011; Williams et al., 2011, 2014). Loss of Wdr62 was reported to cause cell fate defects in both *Drosophila* and mammalian neural stem cells (Jayaraman et al., 2016; Lim et al., 2017; Ramdas Nair et al., 2016; Xu et al., 2014), but the role of Wdr62 in spindle orientation has yet to be examined in non-neuronal tissue. Given the observed role of JNK in regulating ISC spindle orientation, we tested whether Wdr62 would also influence spindle orientation. Overexpression of Wdr62 in ISCs shifted spindle orientation planar to the basal surface, while depleting Wdr62 by RNAi in ISCs was sufficient to prevent the JNK- or paraquat-induced shift toward planar spindles (in live and fixed tissue) (Figures 4B, 4C, and S6A). Depleting Wdr62 in mock-treated conditions did not significantly change average spindle angles (Figure 4B), suggesting that Wdr62 is specifically engaged to control spindle orientation in conditions that also activate JNK. Consistent with these changes in spindle orientation, the percentage of D1+ cells decreased after Wdr62 depletion in intestines of paraquat-treated animals and increased after Wdr62 overexpression (Figures 4D and 4E). As an alternative strategy to test Wdr62 function, we generated ISC lineages homozygous for a *wdr62* loss-of-function allele ($wdr62^{\Delta 3\text{-}9}$) (Ramdas Nair et al., 2016) using MARCM (mosaic analysis with a repressible cell marker) (Lee and Luo, 2001) and compared spindle orientation between mitotic cells within clones (i.e., Wdr62-deficient ISCs) and outside clones (i.e., wild-type ISCs). After paraquat treatment, spindles from control crosses were largely planar in mitotic cells both inside and outside clones (Figure 4G). In MARCM clones homozygous for $wdr62^{\Delta 3\text{-}9}$, however, spindles were largely oblique even after paraquat exposure, whereas spindle orientation of mitotic ISCs outside of clones in flies of the same genotype shifted planar as expected.

In mouse embryonic neural stem cells, loss of Wdr62 has been reported to cause defects in spindle assembly, in addition to changes in spindle orientation, although its exact role remains controversial (Jayaraman et al., 2016). In the *Drosophila* intestine, spindle assembly was not obviously affected after Wdr62 knockdown (Figure S6E). Furthermore, all observed mitoses in live-imaged guts continued to completion (n = 12 cells) (Video S10), and the number of mitotic cells in whole fixed guts was no different compared with controls (Figure S6D), suggesting that in ISCs, Wdr62 plays a specific role in the orientation of the mitotic spindle. $Wdr62^{RNAi}$ did not seem to cause apoptosis, because the number of cleaved caspase-3+ ISCs did not increase (Figure S6C). Clone sizes from *wdr62* mutant ISCs were reduced compared with controls (Figure S6F), yet it remains unclear whether this is caused by defects in mitotic progression or decreased symmetric fate outcomes.

We then examined the relationship of JNK and Wdr62 at the spindle. Paraquat-mediated accumulation of pJNK at the spindle was not observed in animals expressing Bsk^{DN} or $Wdr62^{RNAi}$ (Figure 5A), while knockdown of *puc* resulted in pJNK localization to the spindle in untreated animals. Similar to pJNK, Wdr62 was present at the spindle after paraquat treatment, but not after *Ecc15* infection (Figure 5B) or in paraquat-exposed animals expressing Bsk^{DN} (Figure 5C). Depletion of Wdr62 also resulted in loss of the Wdr62 signal, confirming the specificity of the antibody (Figure 5C). Furthermore, increasing JNK activity by depletion of Puc was sufficient to promote Wdr62 localization to the spindle. Elevated JNK activity is thus sufficient and required to recruit Wdr62 to the ISC spindle, and phosphorylated JNK and Wdr62 depend mutually on each other for their translocation to the spindle under stress conditions, during which they promote planar spindle orientation.

Mud Is Sequestered from the Cortex in Stressed ISCs

To better understand how JNK regulates spindle orientation, we examined proteins involved in anchoring astral microtubules and thus in linking the spindle with the cell cortex. We tested the role of two such proteins, Pins and Mud (LGN and NuMA in mammals) (Lancaster and Knoblich, 2012; Siller and Doe, 2009). Depleting either Pins or Mud through RNAi increased planar spindles and relative D1+ cell numbers, suggesting that both proteins are required to orient oblique spindles (Figures 4E, 5D, and S6G). Because Mud plays additional roles at the spindle pole during spindle assembly (Bosveld et al., 2017; Du et al., 2002; Izumi et al., 2006; Silk et al., 2009), we expressed GFP-tagged Mud (using a Bac-based transgene in which GFP-tagged Mud is integrated at landing site 50E1, 62E1, and 65B2) (Bosveld et al., 2016) to visualize its localization and differentiate between the two functions of Mud. After inducing a regenerative response by *Ecc15* treatment, we found that 55% of ISCs had Mud

Mean ± SD (A, D, and E); n = 3 samples, with 100 flies per sample (A), and n = 9 flies (D and E), with spindle orientation quantified from ≥25 flies (B and C), 4 flies for Puc^{RNAi} and 6 flies for $Kif1a^{OE}$ (F), or ≥15 flies (G) per condition; N.S., not significant; *p < 0.05, **p < 0.01, ***p < 0.001, based on a Mann-Whitney test (A, F, and G) or Kruskal-Wallis test (B–E). Red bar, mean (B, C, F, and G). Scale bar, 20 μm.
See also Figure S6 and Videos S9 and S10.

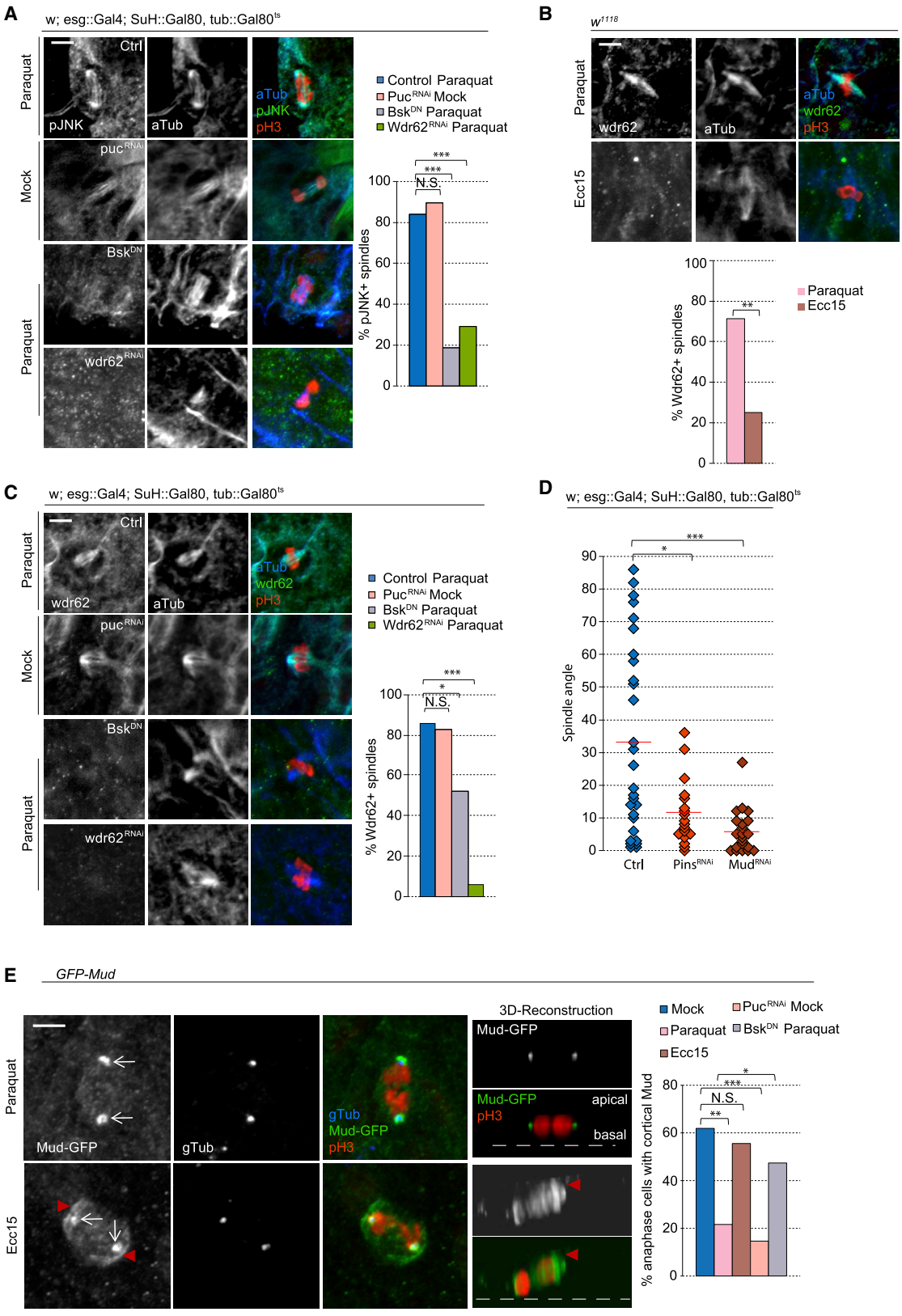

(legend on next page)

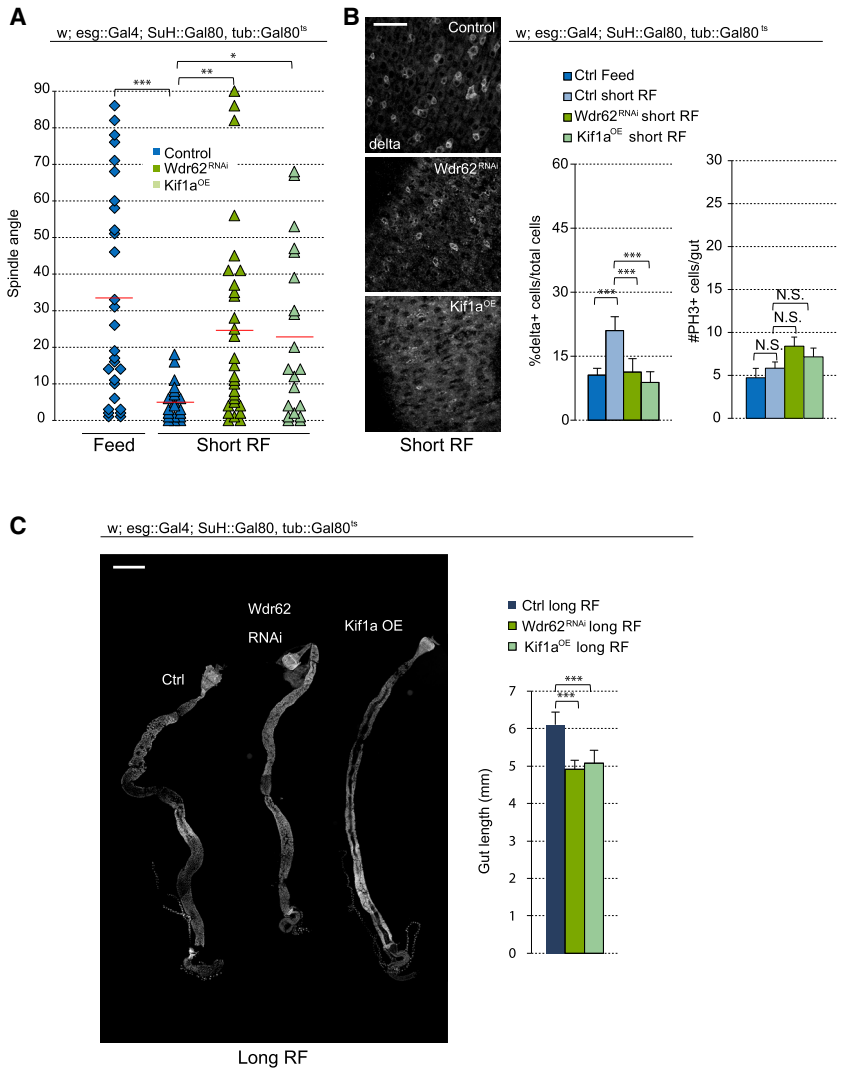

Figure 6. Regulation of Spindle Orientation during Adaptive Growth Depends on Wdr62 and Kif1a

(A) Quantification of spindle orientation after short-term refeeding. Control data for feeding and short-term refeeding were taken from Figure 3B and justified by pooling cells from 18+ flies over 5+ independent experiments.

(B) Percentage of D1+ cells (ISCs) was reduced after Wdr62^{RNAi} or Kif1a overexpression in short-term refed conditions. The number of PH3+ cells in the gut was not affected.

(C) Gut length was decreased after Wdr62^{RNAi} or Kif1a overexpression.

Mean ± SD (B, %D1+ cells, and C) or mean ± SEM (B, #PH3+ cells); n ≥ 9 flies (B, %D1+ cells, and C) and n ≥ 18 flies (B, #PH3+ cells), with spindle orientation quantified from ≥19 flies per condition (A); N.S., not significant; *p < 0.05, **p < 0.01, ***p < 0.001, based on a Kruskal-Wallis test (A–C). Red bar, mean (A). Scale bars, 20 μm (B) and 500 μm (C).

localization at both the spindle pole and the cell cortex (Figure 5E). After paraquat treatment, however, Mud was largely lost from the cell cortex and only localized to the spindle pole, suggesting a potential role for JNK-mediated modulation of Mud localization to promote planar spindles. *puc* depletion was sufficient to cause a loss of cortical Mud in untreated conditions, while Mud was retained at the cell cortex after paraquat treatment when Bsk^{DN} was expressed (Figure 5E). These data suggest that the activity of JNK promotes release of Mud from the cell cortex and thus prevents oblique spindles.

Wdr62 and Kif1a Regulation Is Required for Symmetric Fate Specification during Periods of Growth

Altogether, these results suggest that JNK promotes symmetric divisions by at least two mechanisms: (1) through its direct function at the spindle, where it promotes Wdr62 recruitment and modulates Mud localization, and (2) through its downregulation of Kif1a expression. We asked whether this interaction of JNK with Wdr62 and Kif1a would also be observed during adaptive resizing, a condition that engages JNK activity in a more physiological setting. Similar to Bsk^{DN} expression (Figure 3B), Wdr62 depletion, or Kif1a overexpression, prevented the planar shift of spindles after fasting and short-term refeeding (Figure 6A) and resulted in a lower percentage of D1+ cells compared with controls (Figure 6B). Wdr62 depletion or Kif1a overexpression did not affect the mitotic index during the refeeding process (Figure 6B). We then examined the consequences of preventing symmetric outcomes during

Figure 5. pJNK and Wdr62 Localization to the Spindle Prevents the Recruitment of Cortical Mud

(A) Triple staining with anti-pJNK, anti-phospho-histone H3 (PH3), and anti-α-tubulin to test for pJNK localization at the spindle after genetic perturbations.

(B and C) Triple staining with anti-Wdr62, anti-PH3, and anti-α-tubulin revealed Wdr62 localization at the mitotic spindle after Paraquat treatment (B) or JNK induction (C).

(D) Depletion of Mud and Pins caused a loss of oblique spindles.

(E) Overexpression of GFP-Mud revealed localization at the centrosome (arrow) and the cell cortex (arrowhead). The percentage of anaphase cells with cortical Mud was quantified.

n ≥ 20 cells from ≥12 flies (A, B, C, and E), with spindle orientation quantified from ≥15 flies per condition (D); N.S., not significant; *p < 0.05, **p < 0.01, ***p < 0.001, based on a chi-square test (A, B, C, and E) or Kruskal-Wallis test (D). Red bar, mean (D). Scale bar, 5 μm.

See also Figure S6.

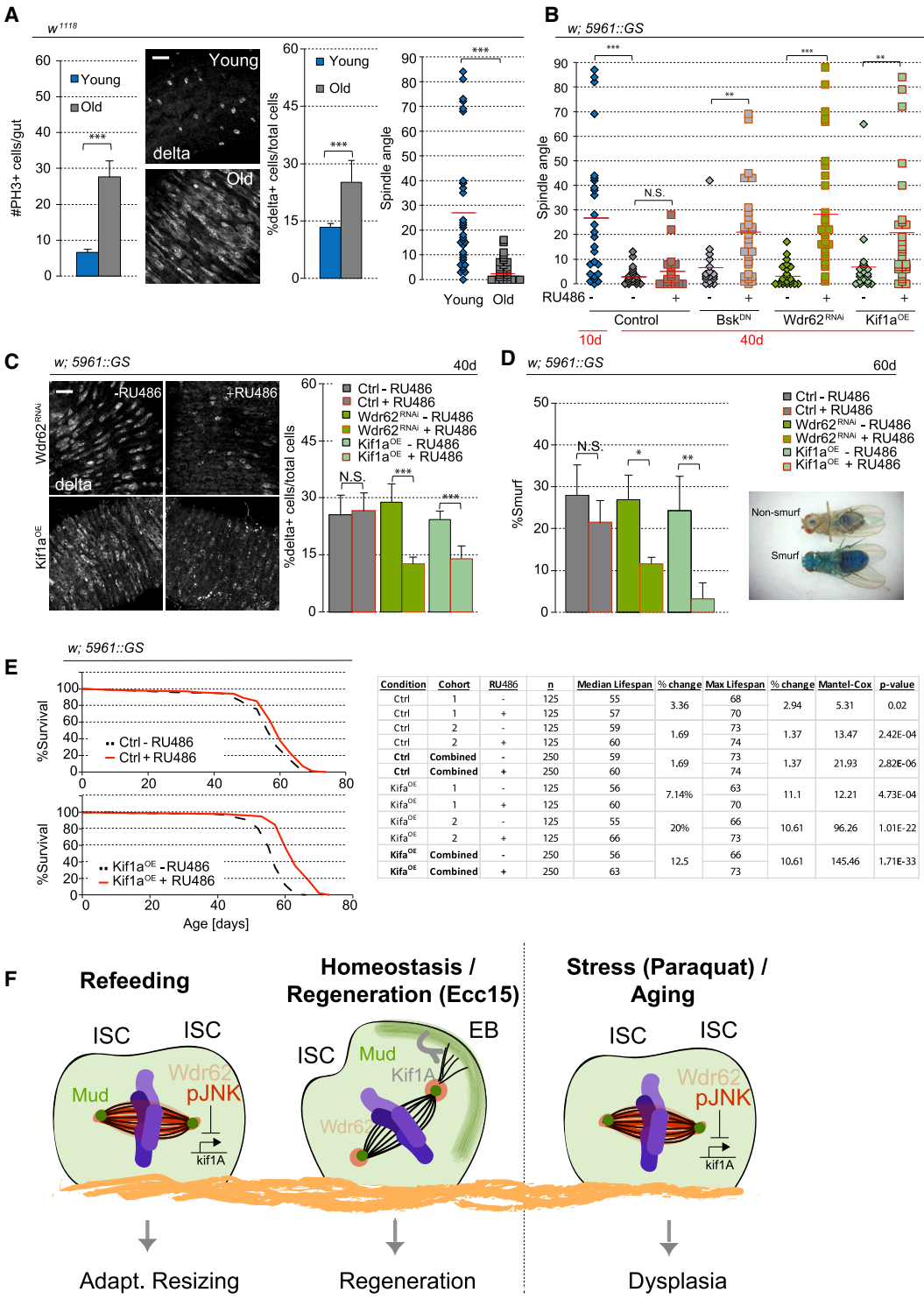

Condition	Cohort	RU486	n	Median Lifespan	% change	Max Lifespan	% change	Mantel-Cox	p-value
Ctrl	1	-	125	55	3.36	68	2.94	5.31	0.02
Ctrl	1	+	125	57		70			
Ctrl	2	-	125	59	1.69	73	1.37	13.47	2.42E-04
Ctrl	2	+	125	60		74			
Ctrl	**Combined**	-	250	59	1.69	73	1.37	21.93	2.82E-06
Ctrl	**Combined**	+	250	60		74			
Kifa^{OE}	1	-	125	56	7.14%	63	11.1	12.21	4.73E-04
Kifa^{OE}	1	+	125	60		70			
Kifa^{OE}	2	-	125	55	20%	66	10.61	96.26	1.01E-22
Kifa^{OE}	2	+	125	66		73			
Kifa^{OE}	**Combined**	-	250	56	12.5	66	10.61	145.46	1.71E-33
Kifa^{OE}	**Combined**	+	250	63		73			

Figure 7. Rescuing Age-Associated Spindle Orientation Defects Restores Intestine Physiology

(A) Mitotic activity, the ratio of D1+ cells, and planar spindles increased in 40-day-old flies. Spindle orientation for young flies was taken from Figure 1H (fed flies), because young and fed flies have the same condition, and data were pooled from 16 flies over 8 independent experiments.

(B) Quantification of spindle orientation. RU486 was fed to 36-day-old flies, and intestines were dissected from 40-day-old flies.

(C) Quantification of the percentage of D1+ cells. RU486 was fed to 36-day-old flies, and intestines were dissected from 40-day-old flies.

(D) RU486, mixed with blue dye no. 1 in normal food, was fed to 30-day-old females continuously. Intestinal barrier function was assayed by the presence of blue dye strictly in the intestine versus the entirety of the fly. Quantification of the ratio of Smurf flies was performed at day 60.

(legend continued on next page)

growth. Because JNK activity plays a role in mitotic entry during stress and growth (Figure 3C) (Wang et al., 2014) and would affect tissue growth regardless of its effect on spindle orientation, we focused on Wdr62 and Kif1a. After subjecting ISCs to Wdr62 knockdown or Kif1a overexpression during the refeeding process, intestines failed to return to normal size, resulting in decreased tissue length compared with controls (Figure 6C).

Spindle Orientation in Aging ISCs Is Chronically Shifted Planar to the Basal Surface

Our results suggest that cell fate decisions in the ISC lineage are altered depending on the mitogenic stimulus: symmetric divisions prevail during growth, whereas asymmetric divisions predominate during regeneration. We hypothesized that this regulation is crucial in maintaining tissue homeostasis. Supporting this view, when ISCs favor symmetric divisions in response to excess stress signals (such as after paraquat treatment), dysplasia is observed (Figure S5C) (Biteau et al., 2008). A similar phenotype is observed in aging animals, in which chronic activation of JNK triggers increased ISC proliferation and mis-differentiation of ISC daughter cells, resulting in increased numbers of Dl+ cells (Guo et al., 2014; Li et al., 2016). This epithelial dysplasia impairs overall metabolism of the fly, disrupts intestinal barrier function, and ultimately shortens lifespan (Biteau et al., 2010; Rera et al., 2012).

Because this age-related dysplasia is reminiscent of the consequences of promoting a planar spindle orientation in ISCs, we asked whether the intestinal epithelium of old animals (40 days) exhibits increased planar spindles. Although the epithelium is more disorganized in the aging animal, the mitotic ISCs, despite being more abundant, still lined the basement membrane, and spindle orientation was easily measurable (Figure S7A). We confirmed that mitotic activity and the percentage of D1+ cells are increased in 40-day-old animals and found that spindle orientation in most ISCs was planar in 40-day-old flies compared with the oblique orientation predominantly found in ISCs of young animals (Figure 7A). We also observed by live imaging a dominance of planar spindles with minimal rotation in old animals (Figure S7B). We performed live lineage tracing and twin-spot analysis in aging animals and confirmed that these changes are associated with increased symmetric outcomes (Figures 2B and S7C). Similar to other conditions that promote planar spindles (paraquat, short-term refeeding, and JNK activation), pJNK localized to the spindle of aging ISCs (Figure S7D). We then tested whether the overactivation of JNK and its downstream effects contributed to excessive symmetric outcomes and expressed Bsk^{DN} in ISCs using the ISC/EB-specific, RU486-inducible, 5961-Geneswitch expression system (Mathur et al., 2010). RU486 did not change spindle orientation in young or old ISCs in wild-type backgrounds, yet after inducing Bsk^{DN} expression at 36 days of age, spindle orientation was rescued in 40-day-old animals (Figure 7B). Similarly, depleting Wdr62 or overexpressing Kif1a was sufficient to rescue spindle orientation defects in old animals. Restoring spindle orientation in old animals was also sufficient to lower the abnormally high percentage of D1+ cells (Figure 7C). Therefore, our data provide evidence that chronic JNK activation, and its interaction with Wdr62 and repression of Kif1a expression, causes aberrant cell fates in the aging intestinal epithelium by promoting planar spindle orientations. Furthermore, successful rescue after only short-term intervention suggests that the defects in spindle orientation are reversible.

Suppressing Chronic Planar Spindle Orientation Extends Tissue Function and Lifespan

As the fly ages, barrier function of the intestine declines, resulting in loss of intestinal integrity and imminent death (Rera et al., 2012). We tested whether maintaining proper cellular composition by modulating spindle orientation would prevent this barrier dysfunction. To visualize the loss of barrier function, flies were fed with a non-absorbable blue dye starting from 30 days of age. In a healthy fly, only the intestine is stained blue, but when barrier function is lost, the entire fly turns blue, a phenotype called Smurf (Rera et al., 2011) (Figure 7D). When Wdr62 depletion or Kif1a overexpression was induced starting at 30 days of age, a significant decrease of Smurf flies was observed by 60 days of age (Figure 7D). RU486-treatment in control flies did not significantly affect the number of Smurf flies.

Because intestinal health strongly influences *Drosophila* lifespan, we examined whether restoring spindle orientation could extend lifespan. Flies were fed RU486 to induce expression starting at 10 days of age, and although RU486 treatment in the control cross caused only minor changes in median lifespan (1.6%), Kif1a expression increased median lifespan by 12% (Figure 7E), comparable to a previously reported 14.5% median lifespan increase after Bsk^{DN} expression (Biteau et al., 2010). However, depletion of Wdr62 inconsistently affected lifespan in different cohorts (Figure S7E).

In the long-lived survivors overexpressing Kif1a, spindle orientation was rescued even at 60 days of age, but the percentage of Smurf flies increased between 60 and 65 days (Figures S7F and S7G). Mitotic activity in the intestine still increased after Kif1a overexpression, likely contributing to the progression of barrier function (Figure S7F). Kif1a overexpression is thus sufficient to restore oblique spindles and asymmetric divisions regardless of age, but evidently, age-related degeneration of the intestinal epithelium through other mechanisms contributes to the loss of barrier function and mortality at older ages.

Altogether, our results show that manipulating spindle orientation is sufficient to delay the loss of tissue homeostasis and

(E) RU486 was fed to 10-day-old females continuously until the end of the analysis. Kif1a expression resulted in a 12% increase in medial lifespan. Statistical analysis is in the chart.

(F) Model of JNK-mediated regulation of spindle orientation through its interaction with Wdr62 to prevent recruitment of cortical Mud, and downregulation of *kif1a* transcript levels.

Mean ± SD (A, %D1+ cells; C; and D) or mean ± SEM (A, #PH3+ cells); n = 9 flies (A, %D1+ cells, and C), n ≥ 20 flies (A, #PH3 cells), and n = 3–4 cohorts, with ≥30 flies per cohort (D) and spindle orientation data collected from 15–25 flies per condition (A, spindle angle, and B); N.S., not significant; *p < 0.05, **p < 0.01, ***p < 0.001, based on a Mann-Whitney test (A–D). Scale bar, 20 μm.

See also Figure S7.

demonstrate the feasibility of perturbing spindle orientation to extend tissue function and increase longevity.

DISCUSSION

Our study directly demonstrates that cell fate and spindle orientation are tightly linked and identifies a function for JNK signaling in promoting symmetric lineages through the realignment of the mitotic spindle. Our data support a model in which the mutual recruitment of phosphorylated JNK (pJNK) and Wdr62 to the spindle, as well as the JNK-dependent transcriptional repression of Kif1a, is required for spindle positioning toward a planar orientation. Because the activation of JNK also prevents cortical localization of Mud, we propose that JNK activity disrupts engagement of the spindle with cortical determinants of spindle orientation and limits the force exerted on astral microtubules by repressing Kif1a expression (Figure 7F).

Cell Fate Regulation by Spindle Orientation

Our live long-term lineage tracing results reveal that planar spindles result in symmetric division outcomes, whereas oblique spindles precede asymmetric outcomes. As such, changes in spindle orientation (after paraquat, short-term refeeding, and age) reflect changes in division modes. Although live imaging is a powerful tool to directly visualize spindle orientation and fate outcomes, the lower resolution compared with fixed imaging could potentially cause a wider error range in spindle angle measurements. Nonetheless, the ability to clearly visualize the vector bisecting the segregation of the two cell bodies during telophase and the vector lining the basal region of neighboring stem cells helps alleviate this issue. Another potential caveat in our analysis is that fates of ISC daughter cells may have been mis-scored because of a delay in Su(H) activation. However, an asymmetric outcome was never observed to derive from planar spindles, and we scored division outcomes as symmetric only if Su(H) activity was not observed at the end of the time-lapse recording, which was ~4 h after Su(H) activation was first observed in divisions with outcomes scored as asymmetric (Figure S4). In paraquat-exposed animals that overexpressed Kif1a in ISCs (Figure 4F), we detected Su(H) expression in outcomes scored as asymmetric at roughly the same time frame as in control conditions, suggesting that stress conditions like paraquat exposure do not grossly perturb regulation of Su(H) expression.

The spindle angle that separates symmetric and asymmetric divisions is ~15°, and it is unclear whether cell fate specification during divisions with spindle orientation around that angle is deterministic or stochastic. A small subset of spindle orientations above 20° (2 of 22 examples) resulted in 2 YFP+ cells rather than 1 YFP+ cell and 1 YFP+/mCherry+ cell. It is possible that these divisions still result in an asymmetric outcome but may have generated an mCherry− EE cell rather than an mCherry+ EB cell. The rare occurrence of these events is consistent with the smaller population of EEs compared with EB/ECs in the intestine (Figure S5A) (Micchelli and Perrimon, 2006), and spindle orientation during EE fate specification may be important to segregate prospero (Guo and Ohlstein, 2015).

Although our results are thus compatible with a deterministic model for cell fate specification, they do not rule out a role for neutral drift. In a neutral drift model, the stem cell pool is maintained by a balance of ISC loss (by generating two differentiated cells) and duplication (de Navascués et al., 2012; Jin et al., 2017). It is unknown how regulation of spindle orientation affects neutral drift and whether spindle orientation differs between divisions leading to two ISCs or two EBs. Addressing these issues will be important for comprehensive understanding of cell fate determination in this system.

The disparity between spindle behaviors after paraquat treatment and those after *Ecc15* infection shows that the nature of the environmental trigger is critical. Although both stresses induce strong proliferative responses, their effects on spindle orientation and the corresponding cell fate outcome are different. Based on our data, this disparity is likely caused by differing levels of JNK activity. JNK is activated by oxidative stress and is thus strongly induced by paraquat exposure (Biteau et al., 2008). *Ecc15* infection, in turn, promotes ISC proliferation by predominantly stimulating JAK/signal transducer and activator of transcription (STAT) activation in ISCs and only transiently activating JNK (Buchon et al., 2009a, 2009b). JNK was shown to be activated immediately after *Ecc15* infection (30 min post-infection), but the genes encoding components of the JNK pathway were no longer upregulated as early as 4 h post-infection (Buchon et al., 2009a, 2009b). These observations are consistent with our analysis 16–20 h post-infection, particularly the absence of phosphorylated JNK at the mitotic spindle in *Ecc15*-infected animals. However, we cannot rule out a possible role of JNK on spindle orientation at earlier time points after infection.

Previous studies have reported that similar to our observations with *Ecc15*, infection of another strain of bacteria, *Pseudomonas entomophila*, largely promoted asymmetric fate outcomes (Jin et al., 2017). However, JNK activity was still detected in the entire gut 2 days post-infection, although the specific cell type (stem cells versus differentiated cells) in which JNK was activated was not examined (Jiang et al., 2009). We do not rule out the possibility that JNK is activated in ISCs after *P. entomophila* infection. The difference in pathology of *P. entomophila*—which is lethal, unlike *Ecc15*—may contribute to a different response in JNK activation. One hypothesis is that although JNK may be activated after *P. entomophila* infection in ISCs, it is not recruited to the mitotic spindle and therefore would not affect spindle orientation. Future studies are needed to test this hypothesis and explore possible mechanisms of a pathogen-specific difference.

Role of JNK and Wdr62 at the Mitotic Spindle

We find that in recruitment to the spindle, pJNK and Wdr62 depend mutually on each other. Although JNK clearly plays a critical role in this process, our data do not rule out a role for other kinases that have been reported to recruit Wdr62 to the centrosome, including Aurora A and Polo-like kinase (Lim et al., 2016, 2017; Miyamoto et al., 2017; Ramdas Nair et al., 2016). Unlike other reports in neural stem cells (Jayaraman et al., 2016; Ramdas Nair et al., 2016), we did not find an obvious role for Wdr62 in maintaining bipolar spindles. Reports have also identified roles for Wdr62 in stabilizing microtubules and centrosomes in interphase neural stem cells (Jayaraman et al., 2016; Ramdas Nair

et al., 2016), and although we did not explore the effects of Wdr62 depletion during interphase, the absence of gross mitotic defects suggests that in *Drosophila* ISCs, Wdr62 may function selectively in spindle orientation. However, we have observed somewhat smaller clone sizes of ISC lineages deficient for Wdr62 and therefore cannot rule out a function for interphase Wdr62. Disruption of Wdr62 activity during interphase may also contribute to the inconsistent effect on lifespan observed after Wdr62 depletion, despite the restoration of oblique spindles in ISCs of old flies.

The consequences of the loss of Pins and Mud seem to vary depending on the tissue: disrupting Pins and Mud in *Drosophila* neuroblasts randomizes the mitotic spindle, but in the mammalian skin, basal stem cells with depleted LGN favor planar spindles, similar to our observations in *Drosophila* ISCs (Siller et al., 2006; Williams et al., 2011). We observe a loss of cortical Mud after JNK activation, supporting the notion that JNK regulates the interaction between the astral microtubules and the cell cortex to promote planar spindles. The extent to which JNK or Wdr62 interacts directly with Mud is an important question for further study.

Role of Kif1a in Asymmetric Divisions

The mechanism by which Kif1a promotes oblique spindle orientation in ISCs is unclear. Khc-73, a kinesin in the same Kinesin-3 family (Hirokawa et al., 2009), is believed to interact with Pins or Disc Large in *Drosophila* S2 cells and neuroblasts to orient astral microtubules to the cell cortex, and Kif1a may play similar roles in ISCs (Johnston et al., 2009; Siegrist and Doe, 2005). Although our data suggest that JNK regulates Kif1a levels transcriptionally, it is possible that JNK also regulates Kif1a at the protein level and may direct its possible interaction with the spindle recruitment machinery.

JNK Activity and Spindle Orientation during Tissue Resizing and Aging

Our data reveal how a physiological role for JNK signaling in regulating spindle positioning during periods of tissue resizing becomes hijacked under stress and age, limiting tissue homeostasis and shortening lifespan. It remains unclear how JNK is activated in ISCs during starvation-refeeding, but insulin signaling has been implicated in promoting symmetric outcomes during adaptive resizing of the *Drosophila* intestine (O'Brien et al., 2011). It will be interesting to test whether insulin signaling and JNK interact to regulate spindle positioning in ISCs, because elevated insulin signaling activity may also contribute to the age-related chronic activation of JNK. The age-related bias toward planar spindle orientations is reminiscent of the changes in spindle orientation of germline stem cells in old male flies (Cheng et al., 2008), and restoring oblique spindle orientation in aged ISCs by increasing Kif1a expression is sufficient to improve intestinal physiology and extend lifespan. Understanding the exact mechanisms and consequences of ISC spindle positioning will be critical to identifying new intervention strategies to allay age-related dysfunction in barrier epithelia.

Such interventions are likely to have significant clinical relevance, because barrier epithelia in mammals regenerate and age through mechanisms that are similar to the *Drosophila* intestinal epithelium (Guo et al., 2014; Haller et al., 2017; Li and Jasper, 2016; Rock et al., 2011; Thevaranjan et al., 2017). However, although SC fate determination by changes in spindle orientation is observed in multiple mammalian tissues during development (Dumont et al., 2015; Lancaster and Knoblich, 2012; Williams and Fuchs, 2013), the extent to which similar mechanisms determine cell fate in adult mammalian tissues is unclear. Mouse ISCs within the adult intestine use different mechanisms to establish cell fate, because spindle orientation is largely planar, and extrinsic cues preferentially differentiate one of the daughter cells (Ritsma et al., 2014; Snippert et al., 2010). In the mouse trachea, however, it has been reported that spindle orientation fluctuates in basal stem cells in response to injury and may affect cell fate specification (Paul et al., 2014). Given the variation in lineage, cell composition, and organization in different adult tissues, it is likely that the importance of spindle orientation in cell specification differs among tissues. Determining the tissues in which spindle orientation is linked with cell fate, and testing whether the role of JNK in the regulation of spindle orientation in these SCs is conserved, will provide important insight into regenerative biology.

STAR★METHODS

Detailed methods are provided in the online version of this paper and include the following:

- KEY RESOURCES TABLE
- LEAD CONTACT AND MATERIALS AVAILABILITY
- EXPERIMENTAL MODEL AND SUBJECT DETAILS
  - Drosophila stocks, culture, and husbandry
- METHOD DETAILS
  - Drosophila Ecc15 infection and Paraquat treatment
  - Drosophila fast and refeeding
  - Drosophila TARGET and Twinspot/MARCM induction
  - Geneswitch induction and SMURF assay
  - Live imaging of Drosophila intestine and timelapse analysis
  - Immunostaining of Drosophila intestine
  - FACs sorting of ISCs and quantitative reverse transcription PCR (RT-qPCR)
  - Microscopy and image analysis
- QUANTIFICATION AND STATISTICAL ANALYSIS
  - Analysis of mitotic cells
  - Cell fate quantification
  - Twinspot analysis and clone size quantification
  - Live imaging analysis
  - Lifespan and Smurf analysis
  - Statistical analysis
- DATA AND CODE AVAILABILITY

SUPPLEMENTAL INFORMATION

Supplemental Information can be found online at https://doi.org/10.1016/j.celrep.2019.08.014.

ACKNOWLEDGMENTS

We thank Drs. Yohanns Bellïache, Sarah Bray, Marek Mlodzik, Xiaohang Yang, Lucy O'Brien, Benjamin Ohlstein, and Clemens Cabernard for flies and reagents and Nathaniel Troup for technical assistance. This project was supported by NIGMS (R01 GM117412) and NIA (R01 AG047497) to H.J. and NIA (F32 AG053050) to D.J.H.

AUTHOR CONTRIBUTIONS

D.J.H. and H.J. conceived the project and wrote the manuscript; D.J.H. performed experiments and analyzed data. Both authors read and approved the final manuscript.

DECLARATION OF INTERESTS

The authors declare no competing interests.

Received: August 14, 2018
Revised: July 9, 2019
Accepted: July 30, 2019
Published: September 10, 2019

REFERENCES

Ayyaz, A., and Jasper, H. (2013). Intestinal inflammation and stem cell homeostasis in aging *Drosophila melanogaster*. Front. Cell. Infect. Microbiol. *3*, 98.

Bardin, A.J., Perdigoto, C.N., Southall, T.D., Brand, A.H., and Schweisguth, F. (2010). Transcriptional control of stem cell maintenance in the *Drosophila* intestine. Development *137*, 705–714.

Bellaïche, Y., Radovic, A., Woods, D.F., Hough, C.D., Parmentier, M.L., O'Kane, C.J., Bryant, P.J., and Schweisguth, F. (2001). The Partner of Inscuteable/Discs-large complex is required to establish planar polarity during asymmetric cell division in *Drosophila*. Cell *106*, 355–366.

Biteau, B., Hochmuth, C.E., and Jasper, H. (2008). JNK activity in somatic stem cells causes loss of tissue homeostasis in the aging *Drosophila* gut. Cell Stem Cell *3*, 442–455.

Biteau, B., Karpac, J., Supoyo, S., Degennaro, M., Lehmann, R., and Jasper, H. (2010). Lifespan extension by preserving proliferative homeostasis in *Drosophila*. PLoS Genet. *6*, e1001159.

Biteau, B., Karpac, J., Hwangbo, D., and Jasper, H. (2011). Regulation of *Drosophila* lifespan by JNK signaling. Exp. Gerontol. *46*, 349–354.

Bogoyevitch, M.A., Yeap, Y.Y., Qu, Z., Ngoei, K.R., Yip, Y.Y., Zhao, T.T., Heng, J.I., and Ng, D.C. (2012). WD40-repeat protein 62 is a JNK-phosphorylated spindle pole protein required for spindle maintenance and timely mitotic progression. J. Cell Sci. *125*, 5096–5109.

Bosveld, F., Ainslie, A., and Bellaïche, Y. (2017). Sequential activities of Dynein, Mud and Asp in centrosome-spindle coupling maintain centrosome number upon mitosis. J. Cell Sci. *130*, 3557–3567.

Bosveld, F., Markova, O., Guirao, B., Martin, C., Wang, Z., Pierre, A., Balakireva, M., Gaugue, I., Ainslie, A., Christophorou, N., et al. (2016). Epithelial tricellular junctions act as interphase cell shape sensors to orient mitosis. Nature *530*, 495–498.

Buchon, N., Broderick, N.A., Chakrabarti, S., and Lemaitre, B. (2009a). Invasive and indigenous microbiota impact intestinal stem cell activity through multiple pathways in *Drosophila*. Genes Dev. *23*, 2333–2344.

Buchon, N., Broderick, N.A., Poidevin, M., Pradervand, S., and Lemaitre, B. (2009b). *Drosophila* intestinal response to bacterial infection: activation of host defense and stem cell proliferation. Cell Host Microbe *5*, 200–211.

Buszczak, M., Paterno, S., Lighthouse, D., Bachman, J., Planck, J., Owen, S., Skora, A.D., Nystul, T.G., Ohlstein, B., Allen, A., et al. (2007). The carnegie protein trap library: a versatile tool for *Drosophila* developmental studies. Genetics *175*, 1505–1531.

Carabalona, A., Hu, D.J., and Vallee, R.B. (2016). KIF1A inhibition immortalizes brain stem cells but blocks BDNF-mediated neuronal migration. Nat. Neurosci. *19*, 253–262.

Cheng, J., Türkel, N., Hemati, N., Fuller, M.T., Hunt, A.J., and Yamashita, Y.M. (2008). Centrosome misorientation reduces stem cell division during ageing. Nature *456*, 599–604.

Cohen-Katsenelson, K., Wasserman, T., Khateb, S., Whitmarsh, A.J., and Aronheim, A. (2011). Docking interactions of the JNK scaffold protein WDR62. Biochem. J. *439*, 381–390.

Costa, M.R., Wen, G., Lepier, A., Schroeder, T., and Götz, M. (2008). Par-complex proteins promote proliferative progenitor divisions in the developing mouse cerebral cortex. Development *135*, 11–22.

de Chaumont, F., Dallongeville, S., Chenouard, N., Hervé, N., Pop, S., Provoost, T., Meas-Yedid, V., Pankajakshan, P., Lecomte, T., Le Montagner, Y., et al. (2012). Icy: an open bioimage informatics platform for extended reproducible research. Nat. Methods *9*, 690–696.

de Navascués, J., Perdigoto, C.N., Bian, Y., Schneider, M.H., Bardin, A.J., Martínez-Arias, A., and Simons, B.D. (2012). *Drosophila* midgut homeostasis involves neutral competition between symmetrically dividing intestinal stem cells. EMBO J. *31*, 2473–2485.

Delwig, A., Bland, C., Beem-Miller, M., Kimberly, P., and Rand, M.D. (2006). Endocytosis-independent mechanisms of Delta ligand proteolysis. Exp. Cell Res. *312*, 1345–1360.

Deng, H., Gerencser, A.A., and Jasper, H. (2015). Signal integration by Ca(2+) regulates intestinal stem-cell activity. Nature *528*, 212–217.

Doe, C.Q., Chu-LaGraff, Q., Wright, D.M., and Scott, M.P. (1991). The prospero gene specifies cell fates in the *Drosophila* central nervous system. Cell *65*, 451–464.

Du, Q., Taylor, L., Compton, D.A., and Macara, I.G. (2002). LGN blocks the ability of NuMA to bind and stabilize microtubules. A mechanism for mitotic spindle assembly regulation. Curr. Biol. *12*, 1928–1933.

Dumont, N.A., Wang, Y.X., von Maltzahn, J., Pasut, A., Bentzinger, C.F., Brun, C.E., and Rudnicki, M.A. (2015). Dystrophin expression in muscle stem cells regulates their polarity and asymmetric division. Nat. Med. *21*, 1455–1463.

Goulas, S., Conder, R., and Knoblich, J.A. (2012). The Par complex and integrins direct asymmetric cell division in adult intestinal stem cells. Cell Stem Cell *11*, 529–540.

Guo, Z., and Ohlstein, B. (2015). Stem cell regulation. Bidirectional Notch signaling regulates *Drosophila* intestinal stem cell multipotency. Science *350*, aab0988.

Guo, L., Karpac, J., Tran, S.L., and Jasper, H. (2014). PGRP-SC2 promotes gut immune homeostasis to limit commensal dysbiosis and extend lifespan. Cell *156*, 109–122.

Haller, S., Kapuria, S., Riley, R.R., O'Leary, M.N., Schreiber, K.H., Andersen, J.K., Melov, S., Que, J., Rando, T.A., Rock, J., et al. (2017). mTORC1 Activation during Repeated Regeneration Impairs Somatic Stem Cell Maintenance. Cell Stem Cell *21*, 806–818.e5.

Hao, Y., Du, Q., Chen, X., Zheng, Z., Balsbaugh, J.L., Maitra, S., Shabanowitz, J., Hunt, D.F., and Macara, I.G. (2010). Par3 controls epithelial spindle orientation by aPKC-mediated phosphorylation of apical Pins. Curr. Biol. *20*, 1809–1818.

Hirokawa, N., Noda, Y., Tanaka, Y., and Niwa, S. (2009). Kinesin superfamily motor proteins and intracellular transport. Nat. Rev. Mol. Cell Biol. *10*, 682–696.

Igaki, T., Pastor-Pareja, J.C., Aonuma, H., Miura, M., and Xu, T. (2009). Intrinsic tumor suppression and epithelial maintenance by endocytic activation of Eiger/TNF signaling in *Drosophila*. Dev. Cell *16*, 458–465.

Izumi, Y., Ohta, N., Hisata, K., Raabe, T., and Matsuzaki, F. (2006). *Drosophila* Pins-binding protein Mud regulates spindle-polarity coupling and centrosome organization. Nat. Cell Biol. *8*, 586–593.

Jasper, H., Benes, V., Schwager, C., Sauer, S., Clauder-Münster, S., Ansorge, W., and Bohmann, D. (2001). The genomic response of the *Drosophila* embryo to JNK signaling. Dev. Cell *1*, 579–586.

Jayaraman, D., Kodani, A., Gonzalez, D.M., Mancias, J.D., Mochida, G.H., Vagnoni, C., Johnson, J., Krogan, N., Harper, J.W., Reiter, J.F., et al. (2016). Microcephaly Proteins Wdr62 and Aspm Define a Mother Centriole Complex Regulating Centriole Biogenesis, Apical Complex, and Cell Fate. Neuron *92*, 813–828.

Jiang, H., Patel, P.H., Kohlmaier, A., Grenley, M.O., McEwen, D.G., and Edgar, B.A. (2009). Cytokine/Jak/Stat signaling mediates regeneration and homeostasis in the *Drosophila* midgut. Cell *137*, 1343–1355.

Jiang, H., Grenley, M.O., Bravo, M.J., Blumhagen, R.Z., and Edgar, B.A. (2011). EGFR/Ras/MAPK signaling mediates adult midgut epithelial homeostasis and regeneration in *Drosophila*. Cell Stem Cell *8*, 84–95.

Jin, Y., Patel, P.H., Kohlmaier, A., Pavlovic, B., Zhang, C., and Edgar, B.A. (2017). Intestinal Stem Cell Pool Regulation in *Drosophila*. Stem Cell Reports *8*, 1479–1487.

Johnston, C.A., Hirono, K., Prehoda, K.E., and Doe, C.Q. (2009). Identification of an Aurora-A/PinsLINKER/Dlg spindle orientation pathway using induced cell polarity in S2 cells. Cell *138*, 1150–1163.

Keyes, B.E., and Fuchs, E. (2018). Stem cells: Aging and transcriptional fingerprints. J. Cell Biol. *217*, 79–92.

Knoblich, J.A., Jan, L.Y., and Jan, Y.N. (1995). Asymmetric segregation of Numb and Prospero during cell division. Nature *377*, 624–627.

Lancaster, M.A., and Knoblich, J.A. (2012). Spindle orientation in mammalian cerebral cortical development. Curr. Opin. Neurobiol. *22*, 737–746.

Lechler, T., and Fuchs, E. (2005). Asymmetric cell divisions promote stratification and differentiation of mammalian skin. Nature *437*, 275–280.

Lee, T., and Luo, L. (2001). Mosaic analysis with a repressible cell marker (MARCM) for *Drosophila* neural development. Trends Neurosci. *24*, 251–254.

Li, H., and Jasper, H. (2016). Gastrointestinal stem cells in health and disease: from flies to humans. Dis. Model. Mech. *9*, 487–499.

Li, H., Qi, Y., and Jasper, H. (2016). Preventing Age-Related Decline of Gut Compartmentalization Limits Microbiota Dysbiosis and Extends Lifespan. Cell Host Microbe *19*, 240–253.

Lim, N.R., Yeap, Y.Y.C., Ang, C.-S., Williamson, N.A., Bogoyevitch, M.A., Quinn, L.M., and Ng, D.C.H. (2016). Aurora A phosphorylation of WD40-repeat protein 62 in mitotic spindle regulation. Cell Cycle *15*, 413–424.

Lim, N.R., Shohayeb, B., Zaytseva, O., Mitchell, N., Millard, S.S., Ng, D.C.H., and Quinn, L.M. (2017). Glial-Specific Functions of Microcephaly Protein WDR62 and Interaction with the Mitotic Kinase AURKA Are Essential for *Drosophila* Brain Growth. Stem Cell Reports *9*, 32–41.

Lucchetta, E.M., and Ohlstein, B. (2017). Amitosis of Polyploid Cells Regenerates Functional Stem Cells in the *Drosophila* Intestine. Cell Stem Cell *20*, 609–620.e6.

Martin, J.L., Sanders, E.N., Moreno-Roman, P., Jaramillo Koyama, L.A., Balachandra, S., Du, X., and O'Brien, L.E. (2018). Long-term live imaging of the *Drosophila* adult midgut reveals real-time dynamics of division, differentiation and loss. eLife *7*, e36248.

Martín-Blanco, E., Gampel, A., Ring, J., Virdee, K., Kirov, N., Tolkovsky, A.M., and Martinez-Arias, A. (1998). puckered encodes a phosphatase that mediates a feedback loop regulating JNK activity during dorsal closure in *Drosophila*. Genes Dev. *12*, 557–570.

Mathur, D., Bost, A., Driver, I., and Ohlstein, B. (2010). A transient niche regulates the specification of *Drosophila* intestinal stem cells. Science *327*, 210–213.

McGuire, S.E., Mao, Z., and Davis, R.L. (2004). Spatiotemporal gene expression targeting with the TARGET and gene-switch systems in *Drosophila*. Sci. STKE *2004*, pl6.

Micchelli, C.A., and Perrimon, N. (2006). Evidence that stem cells reside in the adult *Drosophila* midgut epithelium. Nature *439*, 475–479.

Miyamoto, T., Akutsu, S.N., Fukumitsu, A., Morino, H., Masatsuna, Y., Hosoba, K., Kawakami, H., Yamamoto, T., Shimizu, K., Ohashi, H., and Matsuura, S. (2017). PLK1-mediated phosphorylation of WDR62/MCPH2 ensures proper mitotic spindle orientation. Hum. Mol. Genet. *26*, 4429–4440.

Morin, X., and Bellaïche, Y. (2011). Mitotic spindle orientation in asymmetric and symmetric cell divisions during animal development. Dev. Cell *21*, 102–119.

Morrison, S.J., and Spradling, A.C. (2008). Stem cells and niches: mechanisms that promote stem cell maintenance throughout life. Cell *132*, 598–611.

Nam, H.J., Jang, I.H., You, H., Lee, K.A., and Lee, W.J. (2012). Genetic evidence of a redox-dependent systemic wound response via Hayan protease-phenoloxidase system in *Drosophila*. EMBO J. *31*, 1253–1265.

O'Brien, L.E., Soliman, S.S., Li, X., and Bilder, D. (2011). Altered modes of stem cell division drive adaptive intestinal growth. Cell *147*, 603–614.

Ohlstein, B., and Spradling, A. (2006). The adult *Drosophila* posterior midgut is maintained by pluripotent stem cells. Nature *439*, 470–474.

Ohlstein, B., and Spradling, A. (2007). Multipotent *Drosophila* intestinal stem cells specify daughter cell fates by differential notch signaling. Science *315*, 988–992.

Patel, P.H., Dutta, D., and Edgar, B.A. (2015). Niche appropriation by *Drosophila* intestinal stem cell tumours. Nat. Cell Biol. *17*, 1182–1192.

Paul, M.K., Bisht, B., Darmawan, D.O., Chiou, R., Ha, V.L., Wallace, W.D., Chon, A.T., Hegab, A.E., Grogan, T., Elashoff, D.A., et al. (2014). Dynamic changes in intracellular ROS levels regulate airway basal stem cell homeostasis through Nrf2-dependent Notch signaling. Cell Stem Cell *15*, 199–214.

Ramdas Nair, A., Singh, P., Salvador Garcia, D., Rodriguez-Crespo, D., Egger, B., and Cabernard, C. (2016). The Microcephaly-Associated Protein Wdr62/CG7337 Is Required to Maintain Centrosome Asymmetry in *Drosophila* Neuroblasts. Cell Rep. *14*, 1100–1113.

Rera, M., Bahadorani, S., Cho, J., Koehler, C.L., Ulgherait, M., Hur, J.H., Ansari, W.S., Lo, T., Jr., Jones, D.L., and Walker, D.W. (2011). Modulation of longevity and tissue homeostasis by the *Drosophila* PGC-1 homolog. Cell Metab. *14*, 623–634.

Rera, M., Clark, R.I., and Walker, D.W. (2012). Intestinal barrier dysfunction links metabolic and inflammatory markers of aging to death in *Drosophila*. Proc. Natl. Acad. Sci. USA *109*, 21528–21533.

Ritsma, L., Ellenbroek, S.I.J., Zomer, A., Snippert, H.J., de Sauvage, F.J., Simons, B.D., Clevers, H., and van Rheenen, J. (2014). Intestinal crypt homeostasis revealed at single-stem-cell level by *in vivo* live imaging. Nature *507*, 362–365.

Rock, J.R., Gao, X., Xue, Y., Randell, S.H., Kong, Y.Y., and Hogan, B.L. (2011). Notch-dependent differentiation of adult airway basal stem cells. Cell Stem Cell *8*, 639–648.

Rogers, S.L., Rogers, G.C., Sharp, D.J., and Vale, R.D. (2002). *Drosophila* EB1 is important for proper assembly, dynamics, and positioning of the mitotic spindle. J. Cell Biol. *158*, 873–884.

Shen, C.P., Jan, L.Y., and Jan, Y.N. (1997). Miranda is required for the asymmetric localization of Prospero during mitosis in *Drosophila*. Cell *90*, 449–458.

Siegrist, S.E., and Doe, C.Q. (2005). Microtubule-induced Pins/Galphai cortical polarity in *Drosophila* neuroblasts. Cell *123*, 1323–1335.

Silk, A.D., Holland, A.J., and Cleveland, D.W. (2009). Requirements for NuMA in maintenance and establishment of mammalian spindle poles. J. Cell Biol. *184*, 677–690.

Siller, K.H., and Doe, C.Q. (2009). Spindle orientation during asymmetric cell division. Nat. Cell Biol. *11*, 365–374.

Siller, K.H., Cabernard, C., and Doe, C.Q. (2006). The NuMA-related Mud protein binds Pins and regulates spindle orientation in *Drosophila* neuroblasts. Nat. Cell Biol. *8*, 594–600.

Snippert, H.J., van der Flier, L.G., Sato, T., van Es, J.H., van den Born, M., Kroon-Veenboer, C., Barker, N., Klein, A.M., van Rheenen, J., Simons, B.D., and Clevers, H. (2010). Intestinal crypt homeostasis results from neutral competition between symmetrically dividing Lgr5 stem cells. Cell *143*, 134–144.

Tata, P.R., Mou, H., Pardo-Saganta, A., Zhao, R., Prabhu, M., Law, B.M., Vinarsky, V., Cho, J.L., Breton, S., Sahay, A., et al. (2013). Dedifferentiation of committed epithelial cells into stem cells *in vivo*. Nature *503*, 218–223.

Tetteh, P.W., Basak, O., Farin, H.F., Wiebrands, K., Kretzschmar, K., Begthel, H., van den Born, M., Korving, J., de Sauvage, F., van Es, J.H., et al. (2016). Replacement of Lost Lgr5-Positive Stem Cells through Plasticity of Their Enterocyte-Lineage Daughters. Cell Stem Cell *18*, 203–213.

Thevaranjan, N., Puchta, A., Schulz, C., Naidoo, A., Szamosi, J.C., Verschoor, C.P., Loukov, D., Schenck, L.P., Jury, J., Foley, K.P., et al. (2017). Age-Associated Microbial Dysbiosis Promotes Intestinal Permeability, Systemic Inflammation, and Macrophage Dysfunction. Cell Host Microbe *21*, 455–466.e4.

Tian, H., Biehs, B., Warming, S., Leong, K.G., Rangell, L., Klein, O.D., and de Sauvage, F.J. (2011). A reserve stem cell population in small intestine renders Lgr5-positive cells dispensable. Nature *478*, 255–259.

Venkei, Z.G., and Yamashita, Y.M. (2018). Emerging mechanisms of asymmetric stem cell division. J. Cell Biol. *217*, 3785–3795.

Wang, M.C., Bohmann, D., and Jasper, H. (2003). JNK signaling confers tolerance to oxidative stress and extends lifespan in *Drosophila*. Dev. Cell *5*, 811–816.

Wang, L., Zeng, X., Ryoo, H.D., and Jasper, H. (2014). Integration of UPRER and oxidative stress signaling in the control of intestinal stem cell proliferation. PLoS Genet. *10*, e1004568.

Wang, L., Ryoo, H.D., Qi, Y., and Jasper, H. (2015). PERK Limits *Drosophila* Lifespan by Promoting Intestinal Stem Cell Proliferation in Response to ER Stress. PLoS Genet. *11*, e1005220.

Williams, S.E., and Fuchs, E. (2013). Oriented divisions, fate decisions. Curr. Opin. Cell Biol. *25*, 749–758.

Williams, S.E., Beronja, S., Pasolli, H.A., and Fuchs, E. (2011). Asymmetric cell divisions promote Notch-dependent epidermal differentiation. Nature *470*, 353–358.

Williams, S.E., Ratliff, L.A., Postiglione, M.P., Knoblich, J.A., and Fuchs, E. (2014). Par3-mInsc and Gαi3 cooperate to promote oriented epidermal cell divisions through LGN. Nat. Cell Biol. *16*, 758–769.

Wodarz, A., Ramrath, A., Kuchinke, U., and Knust, E. (1999). Bazooka provides an apical cue for Inscuteable localization in *Drosophila* neuroblasts. Nature *402*, 544–547.

Xu, D., Zhang, F., Wang, Y., Sun, Y., and Xu, Z. (2014). Microcephaly-associated protein WDR62 regulates neurogenesis through JNK1 in the developing neocortex. Cell Rep. *6*, 104–116.

Yan, K.S., Gevaert, O., Zheng, G.X.Y., Anchang, B., Probert, C.S., Larkin, K.A., Davies, P.S., Cheng, Z.F., Kaddis, J.S., Han, A., et al. (2017). Intestinal Enteroendocrine Lineage Cells Possess Homeostatic and Injury-Inducible Stem Cell Activity. Cell Stem Cell *21*, 78–90.e6.

Yu, H.H., Chen, C.H., Shi, L., Huang, Y., and Lee, T. (2009). Twin-spot MARCM to reveal the developmental origin and identity of neurons. Nat. Neurosci. *12*, 947–953.

STAR★METHODS

KEY RESOURCES TABLE

REAGENT or RESOURCE	SOURCE	IDENTIFIER
Antibodies		
Mouse anti-delta	Laboratory of Matthew Rand at University of Rochester	N/A
Mouse anti-prospero	DSHB	Cat#MR1A, RRID:AB_528440
Mouse anti-γ-tubulin	Sigma	Cat#T6557, RRID:AB_477584
Mouse anti-phospho-JNK	Cell Signaling	Cat#9255S, RRID:AB_2307321
Mouse anti-Wdr62	Laboratory of Clemens Cabernard at University of Washington	N/A
Rabbit anti-phospho-histone H3	EMD Millipore	Cat#06-570, RRID:AB_310177
Rabbit anti-cleaved caspase 3	Cell Signaling	Cat#9661, RRID:AB_2341188
Rabbit anti-PDM1	Laboratory of Xiaohang Yang at Zhejiang University	N/A
Rat anti-α-tubulin	Bio-Rad	Cat#MCA78G, RRID:AB_325005
Chemicals, Peptides, and Recombinant Proteins		
Dylight 650 Phalloidin	Cell Signaling	Cat#12956S
Mifepristone (RU486)	Cayman Chemical Co	Cat#10006317
FD&C Blue dye no. 1	Spectrum Chemical MFG Corp	Cat#FD1110
Critical Commercial Assays		
RNeasy Kit	QIAGEN	Cat#74134
iScript cDNA Synthesis Kit	Bio-Rad	Cat#170-8890
Experimental Models: Organisms/Strains		
Drosophila melanogaster w^{1118}	Bloomington *Drosophila* Stock Center	N/A
Drosophila melanogaster UAS::eb1-GFP	Bloomington *Drosophila* Stock Center	BDSC Cat# 35512, RRID:BDSC_35512
Drosophila melanogaster UAS::luciferase RNAi	Bloomington *Drosophila* Stock Center	BDSC Cat# 31603, RRID:BDSC_31603
Drosophila melanogaster UAS::GFP	Bloomington *Drosophila* Stock Center	BDSC Cat# 5431, RRID:BDSC_5431
Drosophila melanogaster UAS:unc-104-GFP.RVB	Bloomington *Drosophila* Stock Center	BDSC Cat#24787, RRID:BDSC_24787
Drosophila melanogaster UAS::unc-104-GFP.RVB	Bloomington *Drosophila* Stock Center	BDSC Cat#24788, RRID:BDSC_24788
Drosophila melanogaster UAS::unc-104 RNAi	Bloomington *Drosophila* Stock Center	BDSC Cat#43264, RRID:BDSC_43264
Drosophila melanogaster UAS::unc-104 RNAi	Bloomington *Drosophila* Stock Center	BDSC Cat#28951, RRID:BDSC_28951
Drosophila melanogaster UAS::mud RNAi	Bloomington *Drosophila* Stock Center	BDSC Cat#38190, RRID:BDSC_38190
Drosophila melanogaster UAS::mud RNAi	Bloomington *Drosophila* Stock Center	BDSC Cat#35044, RRID:BDSC_35044
Drosophila melanogaster UAS::pins RNAi	Bloomington *Drosophila* Stock Center	BDSC Cat#29310, RRID:BDSC_29310
Drosophila melanogaster UAS::pins RNAi	Bloomington *Drosophila* Stock Center	BDSC Cat#53968, RRID:BDSC_53968
Drosophila melanogaster UAS::wdr62 RNAi	Bloomington *Drosophila* Stock Center	BDSC Cat#53242, RRID:BDSC_53242
Drosophila melanogaster UAS::puc RNAi	Vienna *Drosophila* RNAi Center	Transformant ID 3018
Drosophila melanogaster vkg-GFP	Kyoto DGGR	DGGR Cat# 110626, RRID:DGGR_110626
Drosophila melanogaster GFP-Mud[50E1]; GFP-Mud[62E1], GFP-Mud[65B2]	Y. Bellïache	N/A
Drosophila melanogaster Su(H)::mCherry	S. Bray	N/A
Drosophila melanogaster UAS::hep	M. Mlodzik	N/A
Drosophila melanogaster UAS::bsk DN	M. Mlodzik	N/A
Drosophila melanogaster esg::gal4; Su(H)::Gal80, tub::Gal80ts	Wang et al., 2014	N/A
Drosophila melanogaster esg::gal4, UAS::2xeYFP; Su(H)::Gal80, tub::Gal80ts	Wang et al., 2014	N/A

(*Continued on next page*)

Continued

REAGENT or RESOURCE	SOURCE	IDENTIFIER
Drosophila melanogaster hs::FLP; FRT40A, UAS::CD8-GFP, UAS::CD2-mir; tub::gal4	L. O'brien	N/A
Drosophila melanogaster FRT40A, UAS::CD2-RFP, UAS::GFP-mir	L. O'brien	N/A
Drosophila melanogaster hs::FLP; FRT40A, tub::Gal80; tub::Gal4, UAS::GFP	B. Ohlstein	N/A
Drosophila melanogaster UAS::wdr62-mDendra	C. Cabernard	N/A
Drosophila melanogaster Wdr62Δ3-9	C. Cabernard	N/A
Oligonucleotides		
TaqMan Probes Unc-104	Thermo Fisher Scientific	Cat#4351372, Dm01826374_g1
TaqMan Probes Actin5c	Thermo Fisher Scientific	Cat#4331182, Dm02361909_s1
Software and Algorithms		
ImageJ	NIH	https://imagej.nih.gov/ij/
GraphPad Prism	GraphPad	https://www.graphpad.com/scientific-software/prism/
Icy	Institut Pasteur	http://icy.bioimageanalysis.org/

LEAD CONTACT AND MATERIALS AVAILABILITY

This study did not generate new unique reagents. Further information and requests for resources and reagents should be directed to and will be fulfilled by the Lead Contact, Heinrich Jasper (jasperh@gene.com).

EXPERIMENTAL MODEL AND SUBJECT DETAILS

Drosophila stocks, culture, and husbandry

The following UAS lines were obtained from the Bloomington *Drosophila* Stock Center: w^{1118}, *eb1-GFP* (35512), *luciferase* RNAi (31603), *GFP* (5431), *kif1a* FL (24787, 24788), *kif1a* RNAi (43264, 28951), *mud* RNAi (35044, 38190), *pins* RNAi (29310, 53968), and *wdr62* RNAi (53242). Lines 28951, 38190, and 53968 were only used for Figure S6G while line 24788 (consisting of the identical transgene as 24787) was only used for Figure 4C. The following UAS line was obtained from the Vienna *Drosophila* Stock Center: *puc* RNAi (v3018). The following line was obtained from the Kyoto *Drosophila* Stock Center: *vkg-GFP* (110626). The following lines were gifts: *GFP-Mud* (Dr. Yohanns Bellïache), *Su(H)::mCherry* (Dr. Sarah Bray), *hep* FL (Dr. Marek Mlodzik), *bsk* DN (Dr. Marek Mlodzik), *esg::gal4; Su(H)::Gal80, tub::Gal80^{ts}* (Wang et al., 2014), *esg::gal4, UAS::2xeYFP; Su(H)::Gal80, tub::Gal80^{ts}* (Wang et al., 2014), *hs::FLP; FRT40A, UAS::CD8-GFP, UAS::CD2-mir; tub::gal4* (Dr. Lucy O'Brien), *FRT40A, UAS::CD2-RFP, UAS::GFP-mir* (Dr. Lucy O'Brien), *hs::FLP; FRT40A, tub::Gal80; tub::Gal4, UAS::GFP* (Dr. Benjamin Ohlstein), *UAS-wdr62::mDendra2* (Dr. Clemens Cabernard), and *wdr62$^{\Delta 3\text{-}9}$* (Dr. Clemens Cabernard). The genotype of flies used in each figure is detailed in Table S1.

Flies for non-TARGET experiments were maintained at 25°C and 65% humidity, on a 12-hour light/dark cycle. TARGET experiments described in Method details. Standard fly food was prepared with the following recipe: 1 l distilled water, 7.3 mL of EtOH, 13 g agar, 22 g molasses, 65 g malt extract, 18 g brewer's yeast, 80 g corn flour, 10 g soy flour, 6.2ml propionic acid, and 2g methyl-p-benzoate. Flies were manipulated by CO^2 anesthesia. Only female flies were used in this study because females exhibit higher intestinal turnover rates than males. All flies were dissected at 10d except for fast/refeeding and aging experiments (detailed below and/or in Figure Legends).

METHOD DETAILS

Drosophila Ecc15 infection and Paraquat treatment

For Paraquat treatment, flies were starved for two hours before fed 5mM Paraquat in 5% sucrose on a vial containing Whatman filter paper for 20 hours, and intestines subsequently dissected. For Ecc15 infection, Ecc15 was cultured in 15ml of LB medium for 16 hours at 30°. The culture was pelleted, resuspended in 5% sucrose in water, and fed to two-hour starved flies for 16-20 hours. Intestines were subsequently dissected. For mock controls, flies were starved for two hours and fed 5% sucrose on a vial containing Whatman filter paper for 20 hours.

Drosophila fast and refeeding

For fast and refeed experiments, 3d flies were fasted in 1% sucrose in water for one week, before returning to standard fly food for 3-7 days as noted (Figure 1B).

Drosophila TARGET and Twinspot/MARCM induction

Flies for TARGET experiments were raised at 18°C (instead of 25°C) and, to induce genetic expression, flies were shifted to 29°C for three days before Paraquat treatment or *Ecc15* infection, or a day before refeeding in fast/refeed experiments (for a total of ~four days induction). Otherwise, flies were shifted from 18°C to 29°C for four days. For activation of Twinspot and MARCM clones, flies were incubated at 37° for 45 minutes. Flies were Paraquat-treated, Ecc15-infected, or fast/refed as described above just prior to heat shock. Twinspot analsysis was performed two to three days post heat shock. For MARCM clones, spindle orientation and clone size was quantified seven days post heat shock with Paraquat treatment performed a day before analyses.

Geneswitch induction and SMURF assay

For Geneswitch experiments, 200μM RU486 was added to standard food. For Smurf experiments, 500mg/ml of FD&C Blue dye no. 1 (Spectrum Chemical MFG Corp) was additionally added. Time point of addition is dependent on experiment, detailed in the Results and Figure Legends. For lifespan and Smurf experiments, 100-125 and 30-50 female flies were respectively housed together per bottle and flipped three times a week.

Live imaging of Drosophila intestine and timelapse analysis

Intestines from adult female flies were dissected in culture media containing 2mM $CaCl_2$, 5mM KCl, 5mM HEPES, 8.2mM $MgCl_2$, 108mM NaCl, 4mM $NaHCO_3$, NaH_2PO_4, 10mM sucrose, 5mM trehalose, and 2% fetal bovine serum (Adult Hemolymph-like Saline, AHLS). Intestines were transferred to a 35mm glass bottom dish (MatTek, P35G-1.5-14-C), embedded in 4% low melting agarose (in AHLS), and submerged in AHLS. The posterior midgut was imaged either at intervals of 10 min for two hours or 10-15 min for 10-15 hours (long-term lineage tracing) on a Yokogawa CSU-W1/Zeiss 3i Marianas spinning disk confocal microscopy system. For the long-term lineage tracing experiments, the 568 channel was not imaged for up to two hours to reduce the effects of any possible phototoxicity.

Immunostaining of Drosophila intestine

Intestines from adult female flies were dissected in PBS (Phosphate-buffered saline, pH 7.4) and fixed for 25 minutes at room temperature in media containing 100mM glutamic acid, 25mM KCl, 20mM $MgSO_4$, 4mM sodium phosphate, 1mM $MgCl_2$, and 4% formaldehyde. Intestines were washed with PBS and stained in PBS, 0.3% Triton X-100 supplemented with 5% donkey serum. Intestines were incubated in primary antibody overnight at 4°C antibody, washed in PBS +0.01% Tween-20, and incubated in secondary antibodies, Phalloidin (1:400), and Hoechst stain (1:1000) for 2 hours at room temperature. For Delta staining, dissected intestines were incubated for ten minutes at room temperature in 100mM glutamic acid, 25mM KCl, 20mM $MgSO_4$, 4mM sodium phosphate, 1mM $MgCl_2$, and 4% formaldehyde, followed by 100% MeOH for five minutes at room temperature. Intestines were washed with 50% MeOH in PBS for two minutes, followed by PBS for five minutes. Immunostaining proceeded as described above.

Antibodies used in this study: Mouse monoclonal against Delta (gift from Dr. Matthew Rand)(Delwig et al., 2006), Prospero (DHSB, MR1A, RRID:AB_528440), γ-tubulin (Sigma, T6557, RRID:AB_477584), phospho-JNK (Cell Signaling, 9255S, RRID:AB_2307321), and Wdr62 (gift from Dr. Clemens Cabernard); rabbit polyclonal against phospho-Histone H3 (EMD Millipore, 06-570, RRID:AB_310177), Cleaved Caspase-3 (Cell Signaling, 9661, RRID:AB_2341188), and Pdm1 (gift from Dr. Xiaohang Yang); and rat monoclonal against α-tubulin (Bio-Rad MCA78G, RRID:AB_325005). Secondary antibodies were cyanine dyes from Jackson ImmunoResearch Laboratories.

FACs sorting of ISCs and quantitative reverse transcription PCR (RT-qPCR)

w1118 or UAS-puc^{RNAi} flies were crossed to flies with nls-GFP expressing ISCs. Dissected intestines (100 per sample) were collected in 5% FBS in PBS on ice and treated with trypsin for 1 hr at 29°, followed by tituration to dissociate tissue. Cells were washed and resuspended in 5% FBS in PBS and GFP+ cells were sorted. RNA was extracted utilizing the RNeasy kit (QIAGEN 74134) and converted to cDNA utilizing the iScript cDNA Synthesis kit (Bio-Rad 170-8890), according to manufacturers' instructions. RT-qPCR was performed with cDNAs from ISCs from three populations (100 flies each) of controls and puc^{RNAi} expressing flies each on a QuantStudio 8 Flex system (ThermoFischer), using TaqMan Probes (ThermoFischer): Kif1a/unc-104 (Dm01826374_g1) and Actin5c (Dm02361909_s1). For data analysis, C(t) values of Kif1a levels in linear scale were normalized to Actin5c.

Microscopy and image analysis

Images were taken either with the Zeiss LSM 700 scanning confocal microscopy system, the Leica SP8 STED 3X scanning confocal microscopy system, or the Yokogawa CSU-W1/Zeiss 3i Marianas spinning disk confocal microscopy system. Intestines were imaged using a 10x PlanFleur, or 40x PlanFleur, or 100x STED objective. 3-D reconstruction was performed using Icy (Quantitative Image Analysis Unit, Institut Pasteur, France) (de Chaumont et al., 2012). Images were analyzed and processed using ImageJ (NIH, Bethesda, MD) and Adobe Photoshop. Figures were composed in Adobe Illustrator. Except for mitotic guts, in which quantification took place in the entire gut, only the posterior midgut was analyzed.

QUANTIFICATION AND STATISTICAL ANALYSIS

All quantifications were performed manually using ImageJ software (NIH, Bethesda, MD). Except for quantification of PH3+ cells, which was performed in the entire gut, only the posterior midgut was analyzed.

Analysis of mitotic cells

Intestines were dissected from females at 10d of age, except for old animals, which were at 40d, and short-term and long-term refed animals (Figure 1B). Mitotic numbers were counted from the entire gut as determined by phospho-histone H3 positivity. Spindle orientation was quantified by measuring the angle between the mitotic spindle (as estimated by α-tubulin staining, γ-tubulin staining, or the vector bisecting the two segregating chromosomes as determined by PH3 staining), with the basement membrane (as determined by Phalloidin). Spindle orientation was only measured from anaphase cells in the posterior midgut. Localization of phospho-JNK and Wdr62 at the spindle was determined by α-tubulin co-staining, and localization of Mud at the spindle pole versus cell cortex was determined by γ-tubulin co-staining. Mud localization was only quantified in anaphase cells in the posterior midgut, while JNK and Wdr62 localization analyses were pooled from metaphase and anaphase ISCs in the posterior midgut. For measurement of phosphorylated JNK (pJNK), fluorescent intensity of pJNK and α-tubulin were set to the same baselines across all images. Relative pJNK levels were measured by normalizing the mean fluorescent intensity of pJNK in an area outlining the spindle with the mean fluorescent intensity of α-tubulin. Relative pJNK levels were also measured in the same area within the nearest non-mitotic cell as comparison.

Cell fate quantification

Cell fate of cells was identified with the following markers: ISCs by Delta staining or fluorophore expression under the control of esg::gal4; Su(H)::Gal80, EBs by Su(H)::mCherry, ECs by pdm1 staining, EEs by prospero staining, and apoptotic cells by cleaved caspase 3 staining. Only the posterior midgut was imaged. The ratio of a given cell fate (i.e., %ISC) was calculated by the percentage of the number of the given cell type over the total number of cells, as determined by DAPI, within a 28.9mm^2 region. Total number of ISCs (#ISCs) was quantified within a 28.9mm^2 region. The percentage of apoptotic ISCs were quantified by the percentage of cleaved caspase 3+ ISCs over total number of ISCs within a 28.9mm^2 region.

Twinspot analysis and clone size quantification

For twinspot analysis, the fate specification of daughter cells from only the first division post induction was scored. Following the first division post induction, a generated ISC will subsequently divide to generate multiple cells of the same color while a generated differentiated cells, if any, no longer divides and does not generate any more cells of the same color. As such, twinspots containing zero or one cell of one color and 2 or more of another were scored as asymmetric while clones with $\geq$ 2 of each color were scored as symmetric. Clones with only one cell of each color were not quantified because it is not clear whether either cell is an EB or an ISC that not yet divided a second time. The number of cells in Twinspot or MARCM clones were quantified using DAPI as a marker. Both Twinspot and MARCM clones were quantified only from the posterior midgut.

Live imaging analysis

Only the posterior midgut was imaged.

For live imaging of spindle orientation with eb1-GFP, spindle orientation was measured during metaphase and anaphase of each mitotic ISC. Mitotic phase was identified by spindle behavior. Spindle orientation was quantified by measuring the angle between the spindle (as determined by eb1-GFP) and basement membrane (estimated by drawing a line along the basal surface of neighboring ISCs).

For cell fate analyses during live imaging, an asymmetric outcome was score when one of the daughter cells became mCherry+. A symmetric outcome was scored when both daughter cells remained mCherry- at the end of a timelapse (generally 11-13 hours post-mitosis). mCherry fluorescent intensity was measured by normalizing the mean fluorescent intensity of the entire cell with the background. During an outcome scored as asymmetric outcome, fluorescent intensity was measured in each daughter cell at the time point of initial visible mCherry fluorescence and at the end of the time point. During an outcome scored as symmetric, fluorescent intensity was measured in each daughter cell at the end of the timelapse and three hours prior. Spindle orientation was quantified by measuring the angle between the vector bisecting the two segregating cell bodies and basement membrane (estimated by drawing a line along the basal surface of neighboring ISCs).

Lifespan and Smurf analysis

For lifespan and Smurf assays, dead/Smurf flies were counted visually every two to three days. Smurf flies were identified by the entire animal turning blue, and were tallied from the day of feeding (day 30) to day of death.

Statistical analysis

Each sample, 'n', is from at least three independent experiments, and is defined in the Figure Legends depending on experiment (generally as flies, cells, or clones). Additional statistical details for each experiment is also noted in the Figure Legends. Statistical

analyses were performed with Prism (GraphPad Software, La Jolla, CA, USA). A Mann-Whitney U test was used to determine statistical significance between two independent groups. A Kruskal-Wallis test was used to determine statistical significance with multiple comparisons between three or more independent groups. A chi-square test was used to test for statistical significance when comparing data according to a set hypothesis (i.e., percentage of spindles with phospho-JNK localization). A log-rank test was used to test for statistical significance in lifespan assays. Significance was accepted at the level of $p < 0.05$. No statistical methods were used to predetermine sample sizes, but our sample sizes are similar to those generally employed in the field. Analyses for mitotic cells were performed on every metaphase/anaphase cells in the posterior midgut. For cell fate, Twinspot/MARCM, and live imaging experiments, the specific region imaged was chosen at random (within the posterior midgut). All experiments (from both live and fixed samples) were quantified blindly.

DATA AND CODE AVAILABILITY

This study did not generate any datasets or code.

Cell Reports, Volume *28*

Supplemental Information

Control of Intestinal Cell Fate by Dynamic Mitotic Spindle Repositioning Influences Epithelial Homeostasis and Longevity

Daniel Jun-Kit Hu and Heinrich Jasper

Figure S1

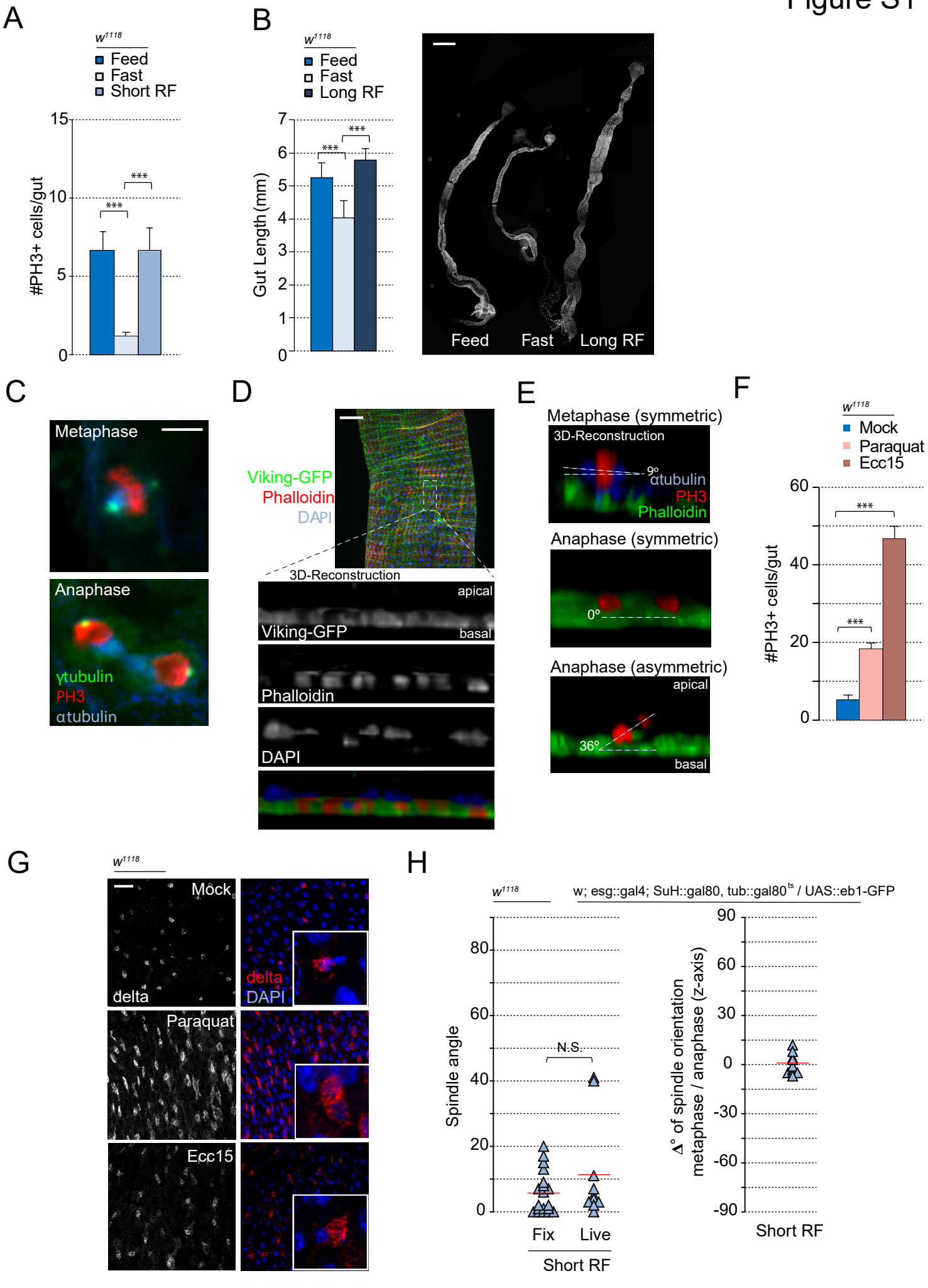
A
w1118
Feed
Fast
Short RF
#PH3+ cells/gut
***
***
B
w1118
Feed
Fast
Long RF
Gut Length (mm)
***
***
Feed
Fast
Long RF
C
Metaphase
Anaphase
γtubulin
PH3
αtubulin
D
Viking-GFP
Phalloidin
DAPI
3D-Reconstruction
apical
Viking-GFP
basal
Phalloidin
DAPI
E
Metaphase (symmetric)
3D-Reconstruction
9°
αtubulin
PH3
Phalloidin
Anaphase (symmetric)
0°
Anaphase (asymmetric)
apical
36°
basal
F
w1118
Mock
Paraquat
Ecc15
#PH3+ cells/gut
***
***
G
w1118
Mock
delta
delta
DAPI
Paraquat
Ecc15
H
w1118
w; esg::gal4; SuH::gal80, tub::gal80ts / UAS::eb1-GFP
Spindle angle
N.S.
Fix
Live
Short RF
Δ° of spindle orientation metaphase / anaphase (z-axis)
Short RF

Figure S1: Visualizing spindle orientation and additional characterization of the *Drosophila* intestine after fasting/refeeding, Paraquat treatment, and *Ecc15* infection, Related to Figure 1.

A. The number of anti-phosphohistone H3+ (PH3) cells in the entire gut decreased after fasting, but recovered after refeeding. B. *Drosophila* intestines substantially decreased in size after fasting, but recover after refeeding. C. Triple staining with anti-γ-tubulin, anti-PH3, and anti-α-tubulin labelling centrosomes and the microtubule network of the mitotic spindle in dividing ISCs. D. 3-D reconstruction of the *Drosophila* intestine to visualize spindle orientation along the apical/basal axis. Fluorescently tagged collagen (Vkg-GFP) or F-actin (Phallodin staining) labeled the basement membrane. E. Spindle orientations were quantified in anaphase ISCs in the posterior midgut by measuring the angle of the line bisecting segregating chromosomes with the basement membrane. F. Mitotic activity of ISCs in the entire gut, as determined by anti-PH3 staining, increased after Paraquat treatment or *Ecc15* infection. G. Representative images of ISCs (as determined by Delta staining) in the posterior midgut after mock or Paraquat treatment, or *Ecc15* infection. Insets depict a likely clone. H. Spindle orientation in live ISCs phenocopied fixed ISCs with a shift to planar spindles. On average, spindle orientation did not change dramatically between metaphase and anaphase. mean ± SD (B) or mean ± SEM (A,F); n≥20 flies (A,F), n≥10 flies (B), spindle orientation was collected from 15 fixed intestines and 6 live intestines (H); N.S. = not significant, ***P<0.001, based on Kruskal-Wallis test (A,B,F), Mann-Whitney test (H). Red bar = mean (H). Scale bar = 500μm (B), 5μm (C), 50μm (D), 20μm (G).

Figure S2

A

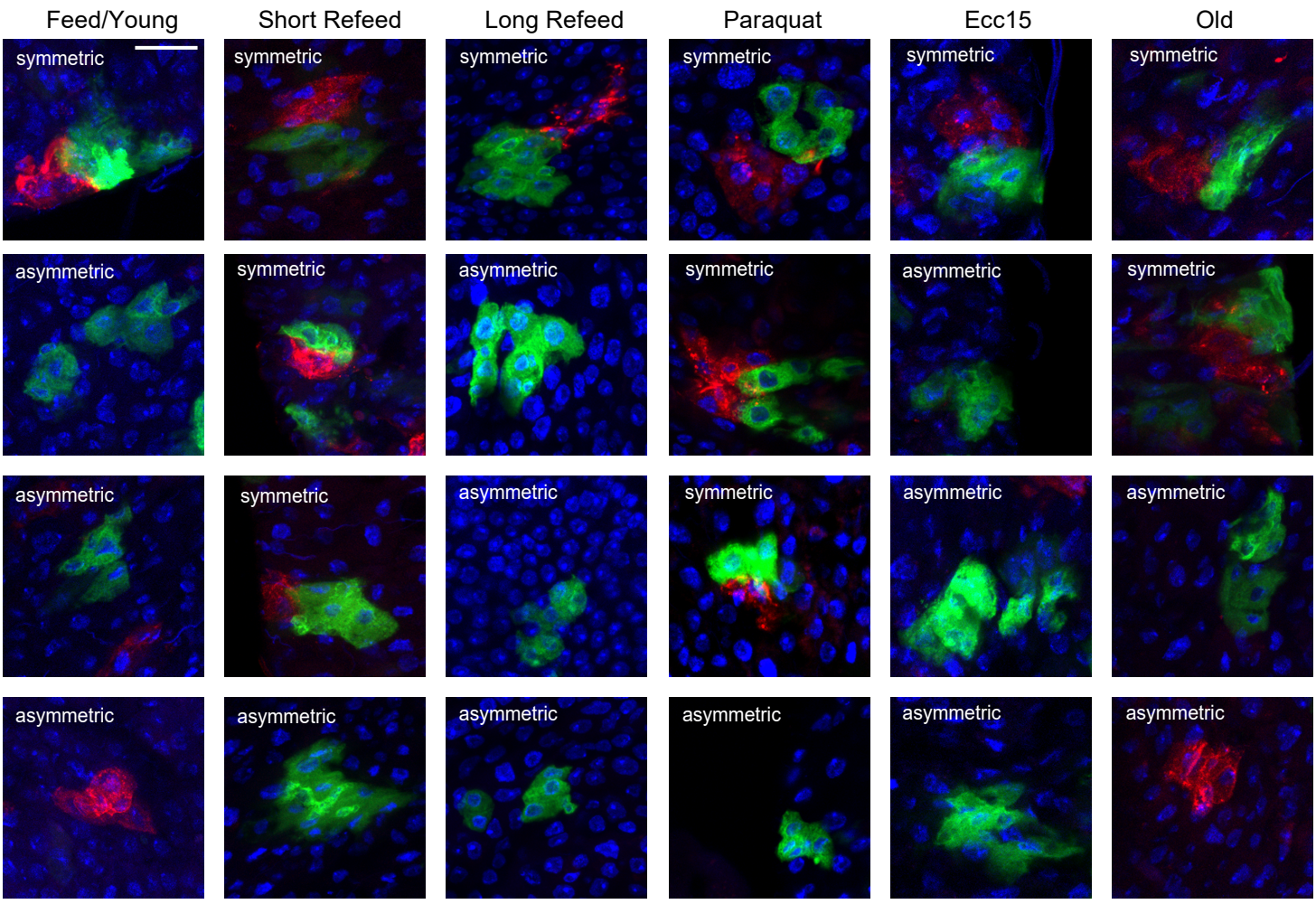

B

	Feed/Young		Short Refeed		Long Refeed		Paraquat		Ecc15		Old	
	#GFP+ Cells	#RFP+ Cells	#GFP+ Cells	#RFP+ Cells	#GFP+ Cells	#RFP+ Cells	#GFP+ Cells	#RFP+ Cells	#GFP+ Cells	#RFP+ Cells	#GFP+ Cells	#RFP+ Cells
Clone 1	0	10	5	27	7	12	4	9	12	0	4	3
Clone 2	7	7	7	11	8	0	37	0	10	0	7	5
Clone 3	8	1	6	9	21	23	7	5	11	0	15	15
Clone 4	9	0	9	5	3	0	9	4	8	0	12	9
Clone 5	10	1	0	7	3	0	5	5	10	6	5	0
Clone 6	0	7	12	5	4	0	20	18	19	1	17	16
Clone 7	0	4	6	3	8	0	43	13	6	0	0	5
Clone 8	6	7	11	5	7	0	3	5	11	1	11	11
Clone 9	8	3	14	0	5	0	5	0	9	0	8	3
Clone 10	8	0	0	8	5	0	6	0	9	4	9	0
Clone 11	5	0	7	3	5	0	4	0	7	11	6	0
Clone 12	6	0	7	6	5	0	5	4	3	3	7	9
Clone 13	5	0	5	7	5	0	7	3	0	4	8	5
Clone 14	7	0	0	14	3	9	27	5	0	8	3	0
Clone 15	8	0	0	13	5	0	0	18	5	0	12	12
Clone 16	8	1	5	3	3	8	5	8	4	0	0	16
Clone 17	9	4	0	7	13	4	16	0	10	5	7	0
Clone 18	7	0	4	4	47	21	21	23	0	7	7	11
Clone 19	4	1	0	5	12	0	4	3	7	3	14	6
Clone 20	4	3	5	5	33	0	17	11	4	0	11	0

Figure S2: Additional Twinspot images and quantification, Related to Figure 2.

A. Examples of Twinspot clones deriving from symmetric or asymmetric fate specifications. B. Quantification of the number of RFP+ and GFP+ in randomly selected clones. n = 20 clones from at least five flies (B). Scale bar = 20μm.

Figure S3

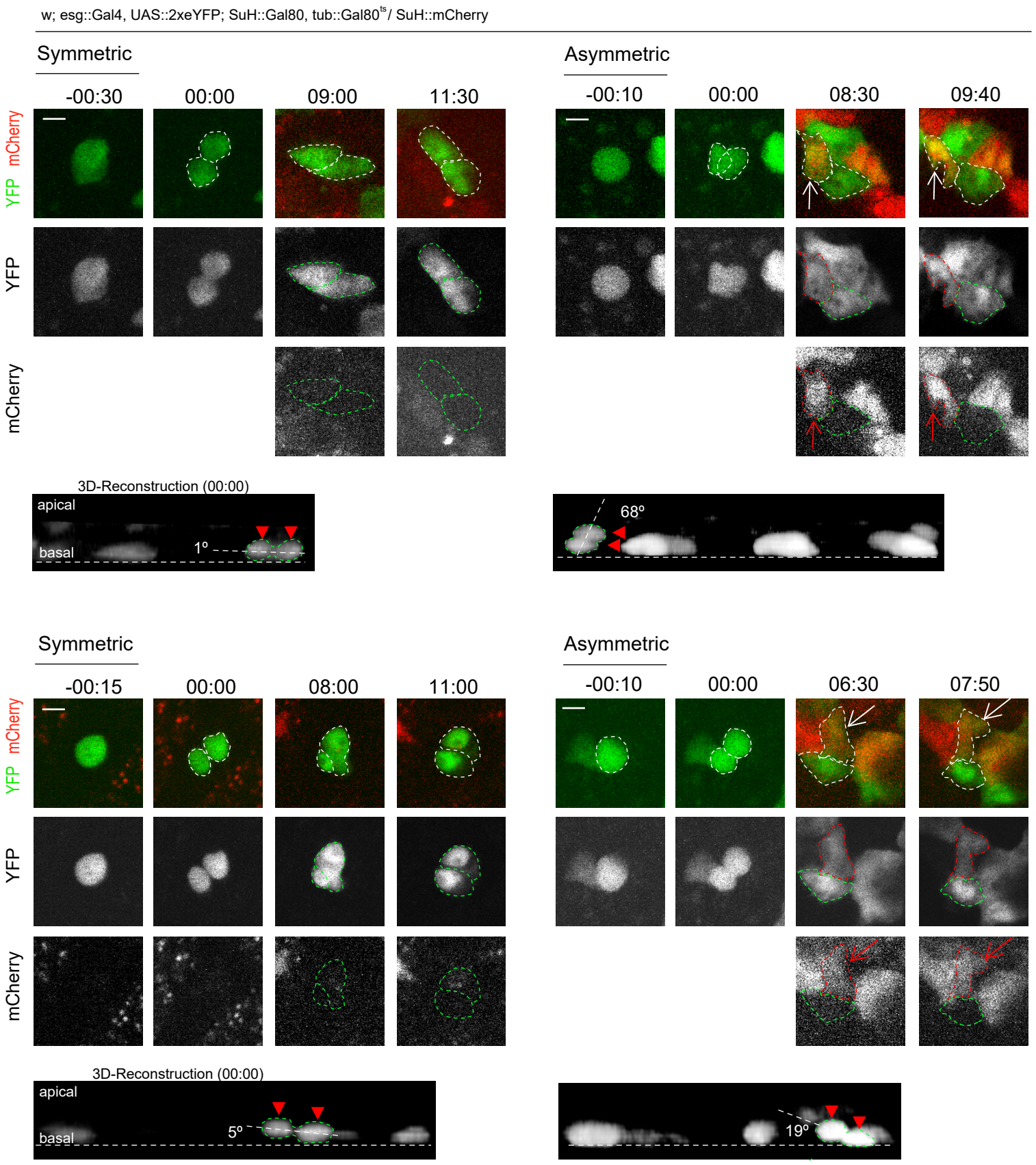
w; esg::Gal4, UAS::2xeYFP; SuH::Gal80, tub::Gal80ts/ SuH::mCherry
Symmetric
-00:30
00:00
09:00
11:30
Asymmetric
-00:10
00:00
08:30
09:40
YFP mCherry
YFP
mCherry
3D-Reconstruction (00:00)
apical
basal
1º
68º
Symmetric
-00:15
00:00
08:00
11:00
Asymmetric
-00:10
00:00
06:30
07:50
YFP mCherry
YFP
mCherry
3D-Reconstruction (00:00)
apical
basal
5º
19º

Figure S3: Additional examples of lineage tracing from long-term live imaging experiments, Related to Figure 2.

Long-term live imaging was performed on *ex vivo* intestines for 10-15 hours, time (hours:minutes). ISCs expressed eYFP while enteroblasts (EBs) expressed mCherry. mCherry was not imaged for the first two hours to reduce phototoxicity. Telophase/cytokinesis was set at 00:00 (hours:minutes). During a symmetric outcome, the dividing cell (-00:30 for example 1; -00:15 – 00:00 for example2) forms two YFP+ mCherry- daughter cells that remain mCherry- for the duration of the movie (11:30 for example 1; 11:00 for example 2). During an asymmetric outcome ,the dividing cell (-00:10 – 00:00) forms two daughter cells: One of the daughter cells remains mCherry- while the other daughter cell becomes mCherry+ (arrow, 08:30 for example 1; 6:30 for example 2). Cell bodies are outlined with green for mCherry- and red for mCherry+. Insets depict 3D-reconstruction of the two segregating cell bodies during telophase/cytokinesis (arrowhead and outlined). The representative symmetric lineages were generated from a planar spindle (1° and 5°) while the representative asymmetric lineages were generated from a more oblique angle (68° and 19°). Scale bar = 5μm.

Figure S4

A

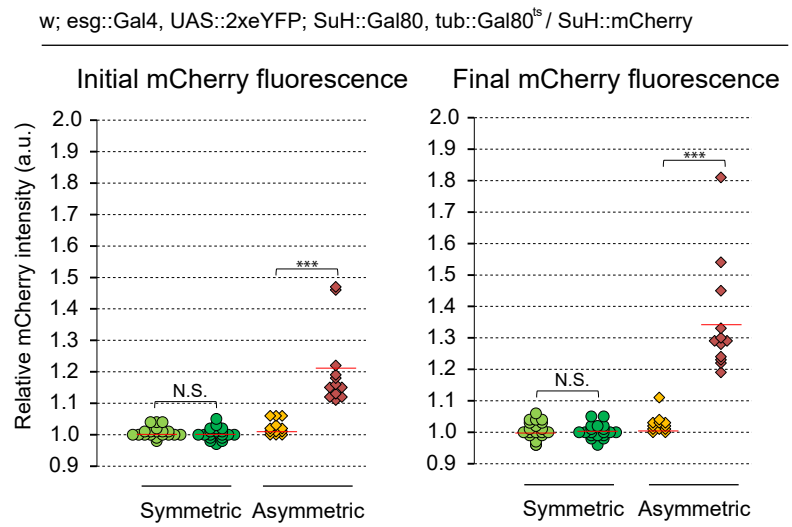

B

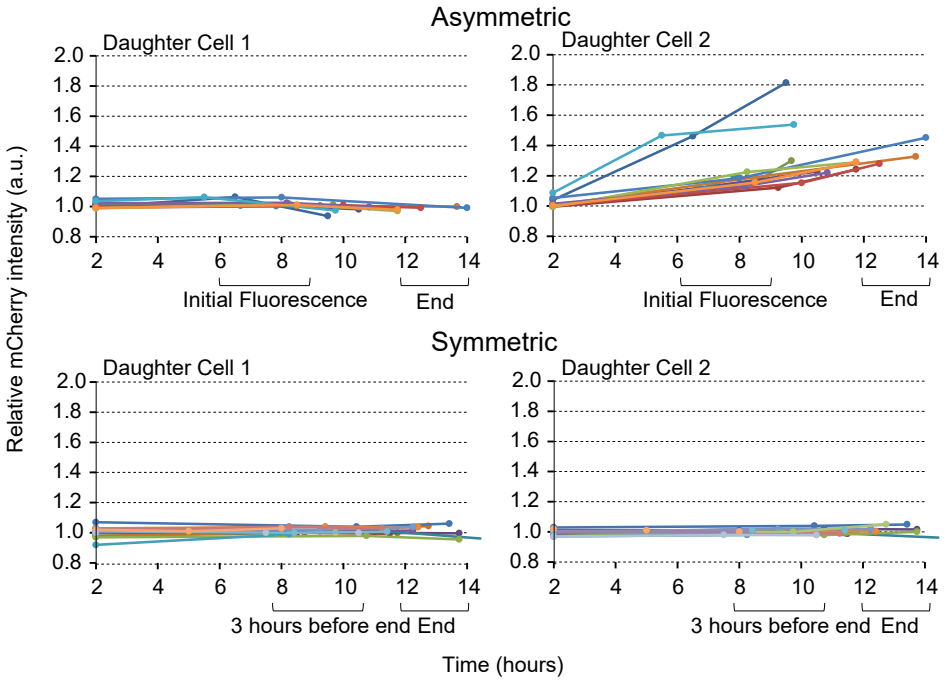

C

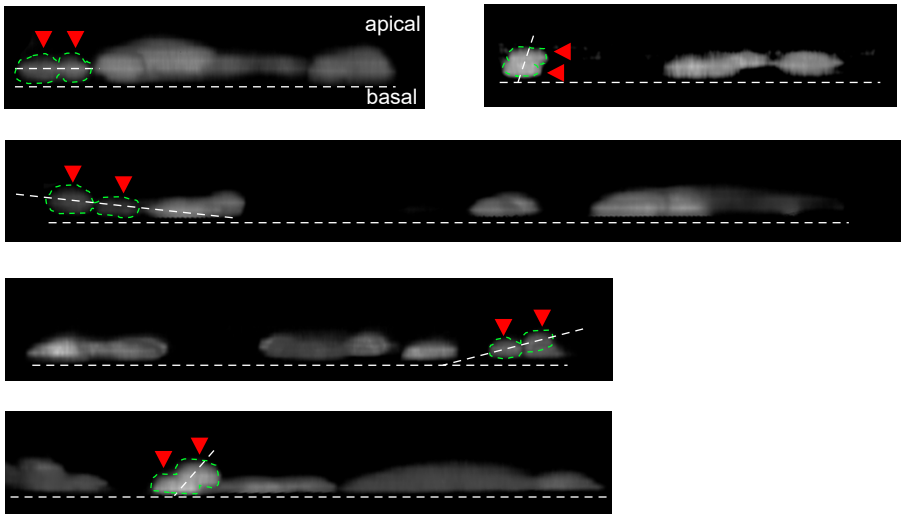

Figure S4: Additional characterization of lineage tracing from long-term live imaging experiments, Related to Figure 2.

Long-term live imaging was performed on *ex vivo* intestines for 10-15 hours to lineage trace cell fates of daughter cells. A. mCherry fluorescence, normalized to background, was measured from both daughter cell pairs (greens and yellow/red) of 31 randomly selected dividing ISCs. During an asymmetric outcome, intensity was measured when fluorescence was first visible (initial mCherry fluorescence; 6-9 hours post mitosis) and at the end of the timelapse (final mCherry fluorescence; generally 11-13 hours post mitosis). High fluorescent intensity was observed in only one of the daughter cell (red). During an outcome scored as symmetric (in which neither cell became mCherry+ at the end of the timelapse), fluorescence was measured at the end of the timelapse (generally 11-14 hours post mitosis) and three hours prior (generally 8-11 hours post mitosis). B. Representation of mCherry fluorescence over time in 31 randomly selected asymmetric versus symmetric outcomes. Each trace represents a daughter cell. C. Additional 3D-reconstruction of dividing ISCs. Spindle angle is measured between the basement membrane estimated by the location of neighboring ISCs and the spindle estimated by the vector bisecting the two segregating cell bodies (green outline and red arrowhead). N.S. = not significant, ***P<0.001, based on Mann-Whitney test (A). Red bar = mean (A).

Figure S5

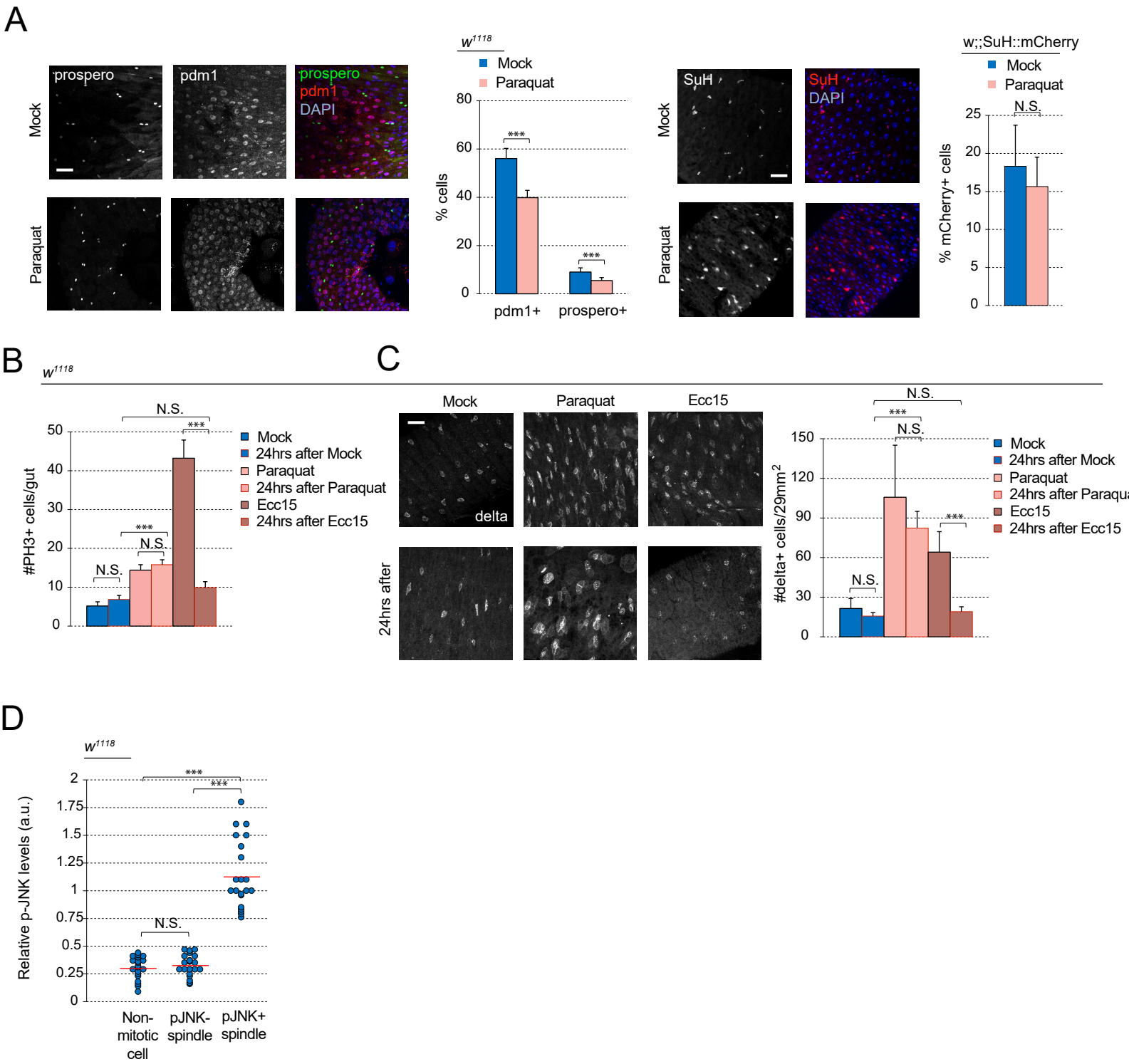
A
prospero
pdm1
prospero
pdm1
DAPI
Mock
Paraquat
w1118
Mock
Paraquat
% cells
pdm1+
prospero+
SuH
SuH
DAPI
w;;SuH::mCherry
% mCherry+ cells
N.S.
B
w1118
#PH3+ cells/gut
Mock
24hrs after Mock
Paraquat
24hrs after Paraquat
Ecc15
24hrs after Ecc15
C
Mock
Paraquat
Ecc15
delta
24hrs after
#delta+ cells/29mm2
D
w1118
Relative p-JNK levels (a.u.)
Non-mitotic cell
pJNK- spindle
pJNK+ spindle

Figure S5: Effects of Paraquat on intestine composition, Related to Figures 3.

A. Paraquat treatment decreased the ratio of enterocytes and enteroendocrine cells (as determined by pdm1 and prospero staining respectively), but did not significantly change the relative number of enteroblasts (as determined by a Su(H)::mCherry reporter). B and C. 8d flies were treated with 5mM Paraquat in 5% sucrose, *Ecc15* in 5% sucrose, or 5% sucrose alone (mock control) for 24 hours, and then transferred to normal food for an additional 24 hours. Flies treated with Paraquat did not recover after 24 hours on normal food, maintaining elevated mitotic activity and ISC number (as determined by PH3 and delta respectively). Flies infected with *Ecc15* recovered completely after 24 hours on normal food, with baseline mitotic activity and ISC numbers. D. Quantification of relative levels of phosphorylated JNK (pJNK) at a randomly selected subset of pJNK- versus pJNK+ spindles. mean ± SD (A,C) or mean ± SEM (B); n=9 flies (A,C), n=15 flies (B), n=21 cells from ≥13 flies (D); N.S. = not significant, ***P<0.001, based on Mann-Whitney test (A,B,C), Kruskal-Wallis test (D). Red bar = mean (D). Scale bar = 20μm.

Figure S6

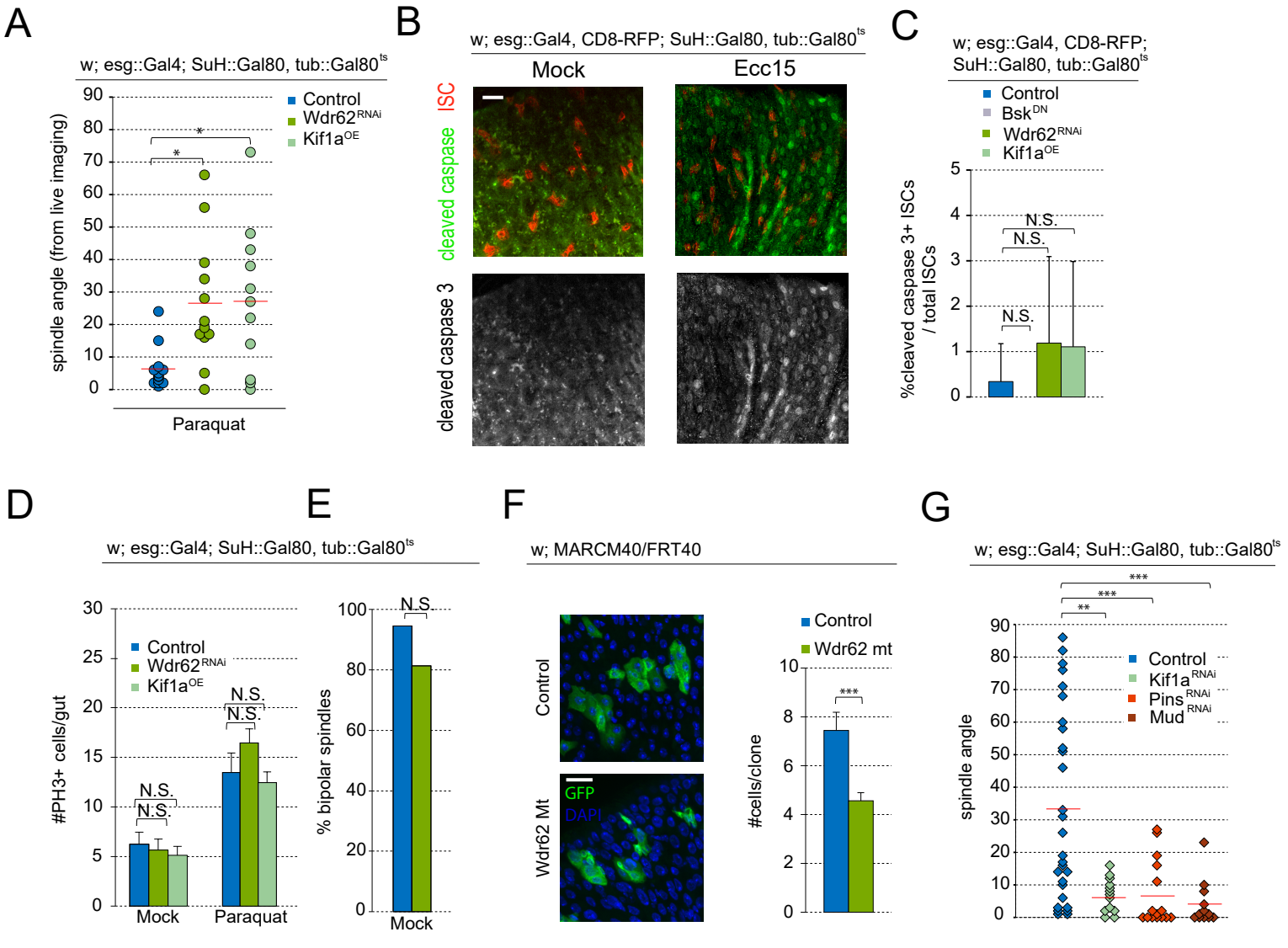

Figure S6: Expression of Wdr62 RNAi and full length Kif1a does not cause apoptosis or block mitosis, Related to Figure 4 and 5.

A. Spindle orientation was quantified by live imaging of *ex vivo* intestines. B. Cleaved caspase 3 staining was validated in *Ecc15*-infected intestine. After 8 hours post infection, many cells were positive for cleaved caspase 3 compared to mock controls. C. Expressing Bsk^{DN}, $Wdr62^{RNAi}$, or full-length Kif1a did not cause apoptosis in ISCs. D. Neither $Wdr62^{RNAi}$ nor $Kif1a^{OE}$ affected the number of PH3+ cells in the whole gut compared to controls. E. $Wdr62^{RNAi}$ did not significantly affect the percentage of bipolar spindles. F. MARCM clones from ISCs homozygous for $wdr62^{\Delta 3\text{-}9}$ are smaller in size than from control ISCs. G. Expression of alternate RNAi against Kif1a, Pins, or Mud also promoted planar spindles. Control data were taken from Figure 3B, justified by the pooling of cells from 25 flies from five independent experiments. mean ± SD (C) or mean ± SEM (D); n=7 flies (C), n≥20 flies (D), n=18 cells from ≥15 flies (E), n≥40 clones from 12 flies (F), spindle orientation was quantified from ≥7 flies (A), ≥10 flies (G); N.S. = not significant, *P<0.05, ***P<0.001, based on Kruskal-Wallis test (A,C,D,G), Chi-Squared test (E), Mann-Whitney test (F). Red bar = mean (D,G). Scale bar = 20μm.

Figure S7

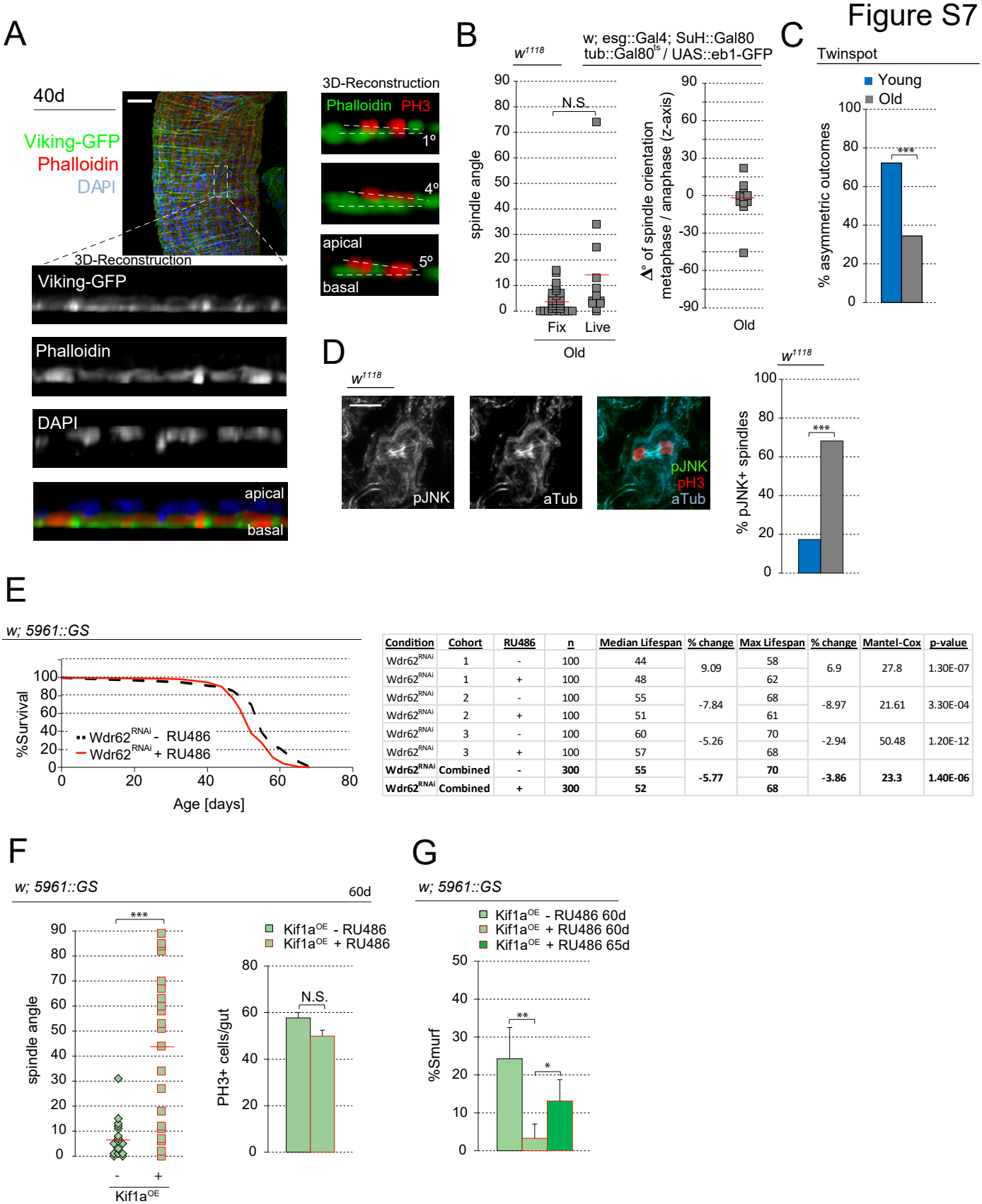

Condition	Cohort	RU486	n	Median Lifespan	% change	Max Lifespan	% change	Mantel-Cox	p-value
Wdr62RNAi	1	-	100	44	9.09	58	6.9	27.8	1.30E-07
Wdr62RNAi	1	+	100	48		62			
Wdr62RNAi	2	-	100	55	-7.84	68	-8.97	21.61	3.30E-04
Wdr62RNAi	2	+	100	51		61			
Wdr62RNAi	3	-	100	60	-5.26	70	-2.94	50.48	1.20E-12
Wdr62RNAi	3	+	100	57		68			
Wdr62RNAi	**Combined**	**-**	**300**	**55**	**-5.77**	**70**	**-3.86**	**23.3**	**1.40E-06**
Wdr62RNAi	**Combined**	**+**	**300**	**52**		**68**			

Figure S7: Additional characterization of spindle orientation in aging ISCs, Related to Figure 7.

A. Spindle orientation is measurable in old flies despite age, with Viking-GFP and Phalloidin still lining the basement membrane. B. Spindle orientation in ISCs from live tissue was not significant different compared to ISCs from fixed tissue. On average, spindle orientation did not change dramatically between metaphase and anaphase. C. Twinspot analysis revealed an increase in symmetric division in old vs young mock-treated ISCs. Old ISCs were from 30d flies as most 40d flies did not survive heat shock. Young flies were taken from Figure 2A as clones were obtained from 10 flies in three independent experiments. D. pJNK localized to the spindle in most old ISCs. E. $Wdr62^{RNAi}$ expression, pooled from three independent experiments (graph), resulted in a modest decrease in lifespan (~6%). Within separate cohorts, $Wdr62^{RNAi}$ expression resulted in substantial increase in lifespan within one cohort, but decreased lifespan within two cohorts (statistical analysis detailed in the chart). RU486 was fed continuously from 10d. F. Spindle orientation remained largely oblique in long-lived survivors (60d) expressing full-length Kif1a. Kif1a expression did not rescue mitotic activity, as determined by PH3 staining. RU486 was fed continuously from 10d. G. Smurf assay was extended to 65d in Kif1a over-expressing flies (RU486 fed to 30d females continuously). %Smurfs increased from 60d to 65d. mean ± SD (C,D,F: spindle angle,G) or mean ± SEM (F: #PH3+ cells); n=133 and 58 clones from 10 young and old flies respectively (C), n=23 cells from 20 flies (D), n= 15 flies (F: #PH3+ cells), n=4 cohorts; ≥ 30 flies per cohort (G), spindle orientation was quantified from 15-18 flies per fixed condition (B, F: spindle angle) and 7 flies for live imaging (B); N.S. = not significant, *P<0.05, **P<0.01, ***P<0.001, based on Mann-Whitney test (B,F), Chi-Squared test (C,D), Kruskal-Wallis test (G). Red bar = mean (B,F: spindle angle). Scale bar = 50μm (A), 5μm (D).